Physica A 603 (2022) 127809

Contents lists available at ScienceDirect

Physica A

journal homepage: www.elsevier.com/locate/physa

Fractal-fractional order dynamics and numerical simulations of a Zika epidemic model with insecticide-treated nets

Emmanuel Addai [a], Lingling Zhang [a,*], Joseph Ackora-Prah [b], Joseph Frank Gordon [c], Joshua Kiddy K. Asamoah [b,*], John Fiifi Essel [a]

[a] Department of Mathematics, Taiyuan University of Technology, Shanxi TaiYuan 030024, PR China
[b] Department of Mathematics, Kwame Nkrumah University of Science and Technology, Kumasi, Ghana
[c] Department of Mathematics Education, Akenten Appiah Menka University of Skills Training and Entrepreneurial Development, Kumasi, Ghana

ARTICLE INFO

Article history:
Received 21 April 2022
Received in revised form 3 June 2022
Available online 23 June 2022

Keywords:
Zika virus
Atangana–Baleanu
Mittag-Leffler kernel
Fractal-fractional derivatives
Newton polynomial
Hyers–Ulam stability

ABSTRACT

Fractional order and fractal order are mathematical tools that can be used to model real-world problems. In order to demonstrate the usefulness of these operators, we develop a new fractal-fractional model for the propagation of the Zika virus. This model includes insecticide-treated nets and the generalized fractal-fractional Mittag-Leffler kernel. The existence, uniqueness, and Ulam–Hyres stability conditions for the given system are determined. Using the Newton polynomial, the numerical scheme is described. From the numerical simulations, we notice that a change in the fractal-fractional order directly affects the dynamics of the Zika virus. We also notice that the use of fractal order only converges to faster than the use of fractional order only. Testing the inherent potency of insecticide-treated nets when the fractal-fractional order is 0.99 indicates that increased use of insecticide-treated nets increases the number of healthy humans. The fractal-fractional analysis captures the geometric pattern of the Zika virus that is repeated at every scale, which cannot be captured by classical geometry. This backs up the idea that the best way to control the disease is to know enough about how it spread in the past.

1. Introduction

The Zika virus, a vector-borne disease initially found in rhesus monkeys in Uganda in 1947, has recently emerged as a severe threat to the global community. It was first detected in humans in 1952 in Uganda and the United Republic of Tanzania [1,2]. There have been Zika virus illness outbreaks in Africa, the Americas, Asia, and the Pacific. Throughout Africa and Asia from the 1960s through the 1980s, uncommon occasional cases of human infection were often followed by moderate sickness [2]. Mild fever, skin rashes, muscle and joint soreness, conjunctivitis, and headaches are among the Zika virus symptoms. On the island of Yap (Federated States of Micronesia), the first Zika virus disease outbreak was reported in 2007 [2]. In 2013, French Polynesia and other Pacific nations and territories saw a large outbreak of Zika virus infection [2]. It was discovered in July 2015 that Zika virus infection was associated with Guillain-Barré syndrome. In March 2015, Brazil reported a large outbreak of rash illness, which was rapidly confirmed as Zika virus infection and linked to Guillain-Barré syndrome in July 2015. In October 2015, Brazil reported a link between Zika virus infection and

* Corresponding authors.
E-mail addresses: papayawewit@gmail.com (E. Addai), tyutzll@126.com (L. Zhang), ackoraprahj@gmail.com (J. Ackora-Prah), topeljoshua@gmail.com, jkkasamoah@kunst.edu.gh (J.K.K. Asamoah).

https://doi.org/10.1016/j.physa.2022.127809
0378-4371/

microcephaly. Rapidly, transmission evidence and epidemics appeared in the Americas, Africa, as well as other regions of the world. Eighty-six countries and territories have reported evidence of Zika virus transmission by mosquitoes (aedes aegypti). In tropical and sub-tropical places in the world, Aedes aegypti causes dengue fever, chikungunya, yellow fever, and Japanese encephalitis [2]. The other means of transmission can be through blood transfusions (very probable but unproven), organ transplants, and sexual contact with a sexual partner [3]. Infected mothers can pass the virus on to their newborns leading to permanent disability. According to the authors of [4], even after the Zika virus has departed from an infected person's blood, it persists in the sperm, adding weight to the theory that it is spread through sexual contact.

As of late, mathematical modelling has been shown to be a very successful tool for monitoring and controlling numerous diseases by providing essential analysis (for example, [5–19]). In the absence of real data, which can be highly expensive, mathematical models provide an alternative platform. The use of mathematical models to forecast the dynamics of disease transmission and to reduce the infection curve has been proposed. In [20], the authors investigated the transmission dynamics of the Zika virus in French Polynesia in 2013–2014. Their model suggested a measurement to protect against future infection. Gonzalez-Parra et al. [21], estimated the subcritical transmissibility of the Zika outbreak in South and North America in 2016. Recently, in [22], the authors formulated a new Zika virus model in light of both mosquito and human transmission along with the human awareness in the host population. Alzahrani et al. [23] used an optimal control approach to study a Zika virus model with mutants. Their results suggested controls to eliminate the virus from the community. In [24], Zika virus model with a sexual transmission route was investigated. Mpeshe et al. [25], formulated a model approach to investigate the dynamics of Zika virus fever in Africa. Bonyah et al. [26], studied the dynamics of Zika virus transmission. They integrated time-dependent controls into the model to evaluate the optimal effects of bednets, infectious illness treatments, and insecticide spraying on the spread of disease. In addition, they utilized Pontryagin's Maximum Principle to calculate the parameters required for efficient disease control and numerical results were provided. Tesla et al. proposed a temperature Zika virus transmission model [27]. They revealed that the expected minimum temperature for Zika transmission is 5 °C higher than that of dengue and that existing global estimates of Zika's environmental adaptability considerably overestimate its potential range. Suparit et al. [28] formulated a mathematical model for Zika virus transmission dynamics with a time-dependent mosquito biting rate. Cai et al. [29] studied the global transmission dynamics of a Zika virus model. Using Lyapunov function they found that the endemic equilibrium point is globally stable. Okyere et al. studied the dynamics of Zika incorporating sexual transmission route together with multiple optimal controls [30]. Fractional calculus has a memory effect, which aids in the correct prediction of physical systems. Some of the fractional order derivatives that have been proposed are Riemann–Liouville–Caputo, Atangana–Baleanu–Caputo (ABC), and Caputo–Fabrizio (CF). The theory of fractional calculus and its illustrated applications are gaining popularity around the world, see the works by [31,32]. New fractional operators with various properties have been defined and are being utilized to model real-world issues. The emergence of novel operators in the literature can be attributed to the replication of new challenges that model various forms of real-world situations. In this regard, many types of fractional operators with varied kernels have been used to solve a range of practical problems, and their numerical methods have been defined in terms of the fractional operators. In the work by [33] the fractional-order biological population model is solved using the natural transform iterative method. The approach addresses a wide variety of fractional and integer-order differential equations. Consideration is given to the fractional-order derivative in Caputo's sense. In [34], the authors investigated a new study on the mathematical modelling of the human liver with CF fractional derivative and concluded that the lower the operator, the infection rate decreases. The authors of [35] investigated the smoke model using the CF fractional derivative and concluded that there is dynamism in hereditary and memory effects in real-world phenomena. The authors in [36] studied the dynamics of Q fever by employing the Mittag-Leffler kernel. They noticed from their studies that, the trajectories of the integer order and some fractional orders converge to the same endemic equilibrium point. Also, they concluded that, as compared to other operators, the ABC fractional differential operator captures greater susceptibilities and fewer infections. Owolabi and Pindza examined a mathematical analysis and numerical treatment for the fractional reaction–diffusion system [37]. The work in [38], studied some chaotic systems using derivative with Mittag-Leffler kernel. In [39], the authors analysed the HIV/AIDS infection model with the Mittag-Leffler kernel where existence–uniqueness, stability, and simulation solutions were established. Furthermore, ABC derivatives have been applied to several contagious diseases such as tuberculosis, smoking epidemics, measles, leptospirosis, COVID-19, etc. [40–50]. The following papers investigated the fractional dynamics of the Zika virus [51–56]. Furthermore, the transmission dynamics of the fractional-order Zika virus in the human population were studied in [57]. In [58], a coupled nonlinear system for Zika virus dynamics with sexual transmission pathway under generalized Caputo-type derivative was investigated. Additionally, in [59], a Mittag-Leffler kernel-based fractional-order Zika virus model was investigated. They showed that the results of their model are more like the results of the traditional model, which is based on Lagrange's interpolation polynomial scheme.

Atangana [60] presented novel operators of differentiation, including the power law convolution, exponential decay law, and modified Mittag-Leffler law with fractal derivative. The novel differential and integral operators are known as fractal-fractional differential and integral operators. The new operators intended to attract a greater number of non-local, fractal-displaying natural challenges. Some additional properties are introduced, along with the numerical approximation of these new operators and their applicability to a real-world scenario. Recently, this fractal-fractional differential and integral operators have been used in studying the complex dynamics of non-infectious and infectious disease (see for

example, [61–71]). Atangana [72] presented fractal-fractional mathematical modelling using differential and integral operators to COVID-19. Detailed descriptions of properties and numerical estimates were provided. Saad et al. [73] studied the fractal-fractional dynamics of hepatitis C virus infection based on Caputo–Fabrizio. They determined the absolute inaccuracy of their solutions, which suggests that the mistake's magnitude diminishes as the number of iterations increases. The chaos of the numerical solutions for the fractal-fractional-order model is depicted graphically for various parameter values. Zhang et al. [74], used a fractal-fractional Caputo derivative to study the dynamics of an anthroponotic cutaneous leishmania model. Their investigation suggests that the fractal-fractional order derivatives provide deeper insight into the intricacy of the suggested Leishmania model's dynamics.

The World Health Organization declared the Zika virus a "Public Health Emergency of International Concern" [2]. Despite the fact that the Zika virus is a public health concern, there is currently no therapy, vaccine, medication, or rapid diagnostic test available, but individuals can avoid mosquito bites [2]. Therefore, based on the fact that fractal-fractional order derivatives provide deeper insight into the intricacy of epidemic models and their ability to capture both memory and heredity traits, and repeated patterns, in this paper, we use fractal-fractional operators to build a model for the Zika virus transmission incorporating insecticide-treated nets, and to the best of our knowledge, no single mathematical formulation of Zika virus transmission in fractal-fractional dynamics has been presented yet. The essential structure of the paper is as follows: We briefly show in Section 2 the fundamental definitions relation to fractal-fractional ABC operators. Construction of the model in classical and fractal-fractional case are respectively shown in Section 3. In Section 4, we analyse the positivity, boundedness and invariant region of the proposed model. The analysis of the existence and uniqueness using fixed point theorem approach are discussed in Section 5. In Section 6 we discussed the stability results under Hyers–Ulam stability. In Section 7, base on Newton polynomial approximation, we analyse the numerical solutions of the fractal-fractional Zika virus transmission incorporating insecticide-treated net. In Section 8, we run a numerical simulation using Matlab to provide a graphical representation of the model. Finally, Section 9 contains the conclusion of the study.

2. Preliminaries

This section contains the basic definitions that will be used throughout the study. These definitions cover the Mittag-Leffler kernel's fractal-fractional derivative in general.

Definition 2.1 ([34]). Given a function $\Upsilon : \mathbb{R}^+ \to \mathbb{R}$, then the fractional integral of order μ_* in Caputo sense is given as

$$ {}_0^C I_\sigma^{\mu_*} \Upsilon(\sigma) = \frac{1}{\Gamma(\mu_*)} \int_0^\sigma (\sigma - \mathfrak{s})^{\mu_* - 1} \Upsilon(\mathfrak{s}) d\mathfrak{s}, \tag{1} $$

where Γ denote the Gamma function and μ_* denote the fractional order.

Definition 2.2 ([75]). Given a function $\Upsilon \in C^n$, then the Caputo derivative with order μ_* is given as

$$ {}_0^C D_\sigma^{\mu_*} \Upsilon(\sigma) = I^{n-\mu_*} D^n \Upsilon(\sigma) = \frac{1}{\Gamma(n-\mu_*)} \int_0^\sigma \frac{\Upsilon^n(\mathfrak{s})}{(\sigma - \mathfrak{s})^{\mu_* + n - 1}} d\mathfrak{s}, \tag{2} $$

which is defined for the continuous functions in absolute terms and $n - 1 < \mu_* < n \in N$. Clearly, ${}_0^C D_\sigma^{\mu_*} \Upsilon(\sigma)$ approaches $\Upsilon'(\sigma)$ as μ_* approaches 1.

Definition 2.3 ([23,76]). Let $\Upsilon \in H^1(a, b)$, $b > a$ be a function and $0 < \mu_* \leq 1$. Then the ABC derivative can be stated as

$$ {}_a^{ABC} D_\sigma^{\mu_*} \Upsilon(\sigma) = \frac{\mathbf{G}(\mu_*)}{1 - \mu_*} \int_a^\sigma \Upsilon'(\mathfrak{s}) E_{\mu_*} \left[-\mu_* \frac{(\sigma - \mathfrak{s})^{\mu_*}}{1 - \mu_*} \right] d\mathfrak{s}, \tag{3} $$

where $\mathbf{G}(\mu_*)$ is a normalization function with $\mathbf{G}(0) = \mathbf{G}(1) = 1$.

$$ E_{\mu_*}(y) = \sum_{k=0}^{\infty} \frac{y^k}{\Gamma(\mu_* k + 1)}, \tag{4} $$

and in a case where we have two parameters Mittag-Leffler function is as follows;

$$ E_{\mu_* \alpha_*}(y) = \sum_{k=0}^{\infty} \frac{y^k}{\Gamma(\mu_* k + \alpha_*)}. \tag{5} $$

Definition 2.4 ([66]). Suppose that $\Upsilon(t)$ is continuous on (a,b) and the fractal-fractional derivative on (a,b) with μ_* and ν_*, as fractal dimension and fractional order respectively, the fractal-fractional (FF) derivative of $\Upsilon(t)$ in Caputo sense with power law-type kernel is given as follows;

$$ {}_0^{FFC} D_\sigma^{\mu_*, \nu_*} \Upsilon(\sigma) = \frac{1}{\Gamma(n-\mu_*)} \int_0^\sigma \frac{d\Upsilon(\mathfrak{s})}{d\mathfrak{s}^{\nu_*}} (\sigma - \mathfrak{s})^{n - \mu_* - 1} d\mathfrak{s}, \tag{6} $$

Table 1
Parameter values and initial conditions.

Parameter	Interpretation	Value/day	Source
Λ_h	Human recruitment rate	100	[26]
Λ_v	Mosquitoes recruitment rate	1000	[26]
ξ_h	Loss of immunity	0.05	Assumed
x_1	Insecticide-treated net coverage	0.1	Assumed
μ_h	Natural death rate for humans	$\frac{1}{60\times 365}$	[26,77]
ϕ_h	Progression of human from exposed to infectious stage	0.01	[26,78]
ϕ_v	Progression of mosquitoes from exposed to infectious stage	0.05	[26]
ν_h	The rate of recovery	0.2	[79]
η_h	Disease-induced death rate for human	0.00001	Assumed
β_h	Probability of humans getting infected	0.2	[78]
β_v	Probability of mosquitoes getting infected	0.09	[77]
μ_v	The death rate of mosquitoes	$\frac{1}{14}$	[79]

where $n-1<\mu_*,\nu_*\leq n\in N$,

$$\frac{d}{ds^{\nu_*}}\Upsilon(\mathfrak{s})=\lim_{\sigma\to\mathfrak{s}}\frac{\Upsilon(\sigma)-\Upsilon(\mathfrak{s})}{\sigma^{\nu_*}-\mathfrak{s}^{\nu_*}} \tag{7}$$

Assume that $\nu_*=1$, then (6) becomes Caputo fractional derivative.

Definition 2.5 ([66]). The fractal-fractional (FF) derivative of $\Upsilon(t)$ in Riemann–Liouville (RL) case with generalized ABC function is given as;

$${}^{FABC}D_{\sigma}^{\mu_*,\nu_*}\Upsilon(\sigma)=\frac{\mathbf{G}(\mu_*)}{1-\mu_*}\frac{d}{d\sigma^{\nu_*}}\int_0^{\sigma}E_{\mu_*}\left(-\mu_*\frac{(\sigma-\mathfrak{s})^{\mu_*}}{1-\mu_*}\right)\Upsilon(\mathfrak{s})d\mathfrak{s}, \tag{8}$$

with $\mu_*>0$, $\nu_*\leq 1\in N$ and $\mathbf{G}(\mu_*)=1-\mu_*+\frac{\mu_*}{\Gamma(\mu_*)}$.

Definition 2.6 ([66]). The fractal-fractional (FF) integral in relation to (8) is as follows;

$${}^{FABC}I_{\sigma}^{\mu_*,\nu_*}\Upsilon(\sigma)=\frac{\nu_*(1-\mu_*)\mathfrak{s}^{\nu_*-1}}{\mathbf{G}(\mu_*)}\Upsilon(\sigma)+\frac{\mu_*,\nu_*}{\mathbf{G}(\mu_*)\Gamma(\mu_*)}\int_0^{\sigma}\mathfrak{s}^{\nu_*-1}(\sigma-\mathfrak{s})^{\mu_*-1}\Upsilon(\mathfrak{s})d\mathfrak{s}. \tag{9}$$

3. Model formulation

Using a system of differential equations, we study human and mosquito populations in a closed homogeneous environment. There are four compartments in a human population of size $N_h(t)$: Susceptible $S_h(t)$; Exposed $E_h(t)$; Infected $I_h(t)$; Recovered $R_h(t)$; where $N_h(t)=S_h(t)+E_h(t)+I_h(t)+R_h(t)$. Due to the facts that only female mosquitoes bite people and transmit Zika virus, the total female mosquitoes population $N_v(t)$ is split into $S_v(t)$ Susceptible; $E_v(t)$ Expose; $I_v(t)$ Infected. Let $N_v(t)=S_v(t)+E_v(t)+I_v(t)$. Note that the mosquito lifespan is usually shorter than their infection period, no recovered mosquitoes are included. From the above description, using the ideas from [23,57], the ordinary differential equations in system (10) describes the Zika virus transmission dynamics incorporating insecticide-treated nets;

$$\begin{cases}\frac{dS_h}{dt}=\Lambda_h+\xi_hR_h-(1-x_1)\lambda_hS_h-\mu_hS_h,\\ \frac{dE_h}{dt}=(1-x_1)\lambda_hS_h-\phi_hE_h-\mu_hE_h,\\ \frac{dI_h}{dt}=\phi_hE_h-(\nu_h+\eta_h)I_h-\mu_hI_h,\\ \frac{dR_h}{dt}=\nu_hI_h-\xi_hR_h-\mu_hR_h,\\ \frac{dS_v}{dt}=\Lambda_v-(1-x_1)\lambda_vS_v-\mu_vS_v,\\ \frac{dE_v}{dt}=(1-x_1)\lambda_vS_v-\phi_vE_v-\mu_vE_v,\\ \frac{dI_v}{dt}=\phi_vE_v-\mu_vI_v,\end{cases} \tag{10}$$

where $\lambda_h=\frac{\beta_hI_v}{N_h}$, $\lambda_v=\frac{\beta_vI_h}{N_h}$. All the parameters in model (10) are summarized in Table 1. The ordinary differential model (10) is then transformed into a fractal-fractional-order system. The reason for addressing the fractal-fractional-order case is the substantial uniqueness of these fractal-fractional-order systems with non-local characteristics, hereditary qualities and repeated patterns that cannot be captured by the used integer-order differential or fractional operators only. The values μ_* and ν_* constitutes the fractional order and the fractal order respectively. In reality, dynamics of diseases can be in a fractal manner, hence integrating fractal perspective would help us comprehend phenomena better. Thus, our

proposed fractal-fractional ABC operator model for Zika virus transmission, which includes insecticide-treated nets is given in Eq. (11).

$$\begin{cases} {}^{FABC}D_t^{\mu_*,\nu_*} S_h(t) = \Lambda_h + \xi_h R_h - (1-x_1)\lambda_h S_h - \mu_h S_h, \\ {}^{FABC}D_t^{\mu_*,\nu_*} E_h(t) = (1-x_1)\lambda_h S_h - \phi_h E_h - \mu_h E_h, \\ {}^{FABC}D_t^{\mu_*,\nu_*} I_h(t) = \phi_h E_h - (\nu_h + \eta_h) I_h - \mu_h I_h, \\ {}^{FABC}D_t^{\mu_*,\nu_*} R_h(t) = \nu_h I_h - \xi_h R_h - \mu_h R_h, \\ {}^{FABC}D_t^{\mu_*,\nu_*} S_v(t) = \Lambda_v - (1-x_1)\lambda_v S_v - \mu_v S_v, \\ {}^{FABC}D_t^{\mu_*,\nu_*} E_v(t) = (1-x_1)\lambda_v S_v - \phi_v E_v - \mu_v E_v, \\ {}^{FABC}D_t^{\mu_*,\nu_*} I_v(t) = \phi_v E_v - \mu_v I_v, \end{cases} \tag{11}$$

with the appropriate non-negative initial conditions as follows; $S_h(0) = S_{h_0} \geq 0$, $E_h(0) = E_{h_0} \geq 0$, $I_h(0) = I_{h_0} \geq 0$, $R_h(0) = R_{h_0} \geq 0$, $S_v(0) = S_{v_0} \geq 0$, $E_v(0) = E_{v_0} \geq 0$, $I_v(0) = I_{v_0} \geq 0$, $T_m(0) = T_{m_0} \geq 0$.

4. Dynamics of the model

In this section, we investigate the dynamics of the positivity, boundedness, and invariant region of the solutions for the proposed model (10) and (11). In an epidemiological model, it is significant to assess the survival of the population and natural restriction to growth due to limited resources. In doing so, we prove the following Theorems.

4.1. Positivity and boundedness

Theorem 4.1. *Let $S_h(0) \geq 0$, $E_h(0) \geq 0$, $I_h(0) \geq 0$, $R_h(0) \geq 0$, $S_v(0) \geq 0$, $E_v(0) \geq 0$, $I_v(0) \geq 0$. Such that the solution set $\Psi = \{S_h(t), E_h(t), I_h(t), R_h(t), S_v(t), E_v(t), I_v(t)\} \in R_+^7$ of the Zika virus model (10) are positive for all $t > 0$. Furthermore*

$$\limsup_{t\to\infty} N_h(t) \leq \frac{\Lambda_h}{\mu_h}, \quad \limsup_{t\to\infty} N_v(t) \leq \left(\frac{\Lambda_v}{\mu_v}\right).$$

Proof. Let $t_1 = \sup\{S_h(0) \geq 0, E_h(0) \geq 0, I_h(0) \geq 0, R_h(0) \geq 0, S_v(0) \geq 0, E_v(0) \geq 0, I_v(0) \geq 0\} \in [0, t]$. We know that the initial values are greater than zero, if not there is nothing to be prove. Therefore, we assume that initial values are greater than zero, then, $t_1 > 0$. Now let take the first dynamical equation of model (10).

$$\frac{dS_h}{dt} = \Lambda_h + \xi_h R_h - (1-x_1)\lambda_h S_h - \mu_h S_h.$$

For simplicity, we let $M_1^* = \left[(1-x_1)\lambda_h - \mu_h\right]$. Thus,

$$\frac{dS_h}{dt} + M_1^* S_h(t) = \Lambda_h + \xi_h R_h.$$

This lead to

$$\frac{d}{dt}\left(S(t)exp\left(\int_0^{t_1} M_1^*(s)ds\right)\right) = \left(\Lambda_h + \xi_h R_h\right)exp\left(\int_0^{t_1} M_1^*(s)ds\right).$$

So, we get

$$S(t) = exp\left(-\int_0^{t_1} M_1^*(s)ds\right)\left[\int_0^{t_1}\left(\Lambda_h + \xi_h R_h\right)exp\left(\int_0^{t_1} M_1^*(s)ds\right)\right].$$

Hence, we proved that $S_h(0) > 0$ for all $t > 0$. In the similar manner, we can prove that $E_h(0) > 0, I_h(0) > 0, R_h(0) > 0, S_v(0) > 0, E_v(0) > 0, I_v(0) > 0$, for all $t > 0$. Now, for boundedness, we have the following expressions as

$$\begin{cases} \frac{dN_h}{dt} = \Lambda_h - \mu_h N_h, \\ \frac{dN_v}{dt} = \Lambda_v - \mu_v N_v. \end{cases} \tag{12}$$

Thus,

$$\Lambda_h - \mu_h N_h \leq \tfrac{dN_h}{dt} \leq \Lambda_h - \mu_h N_h,$$
$$\Lambda_v - \mu_v N_v \leq \tfrac{dN_v}{dt} \leq \Lambda_v - \mu_v N_v.$$

Hence,

$$\liminf_{t\to\infty} N_h(t) \leq \tfrac{\Lambda_h}{\mu_h} \leq \limsup_{t\to\infty} N_h(t) \leq \tfrac{\Lambda_h}{\mu_h},$$
$$\liminf_{t\to\infty} N_v(t) \leq \tfrac{\Lambda_v}{\mu_v} \leq \limsup_{t\to\infty} N_v(t) \leq \tfrac{\Lambda_v}{\mu_v},$$

Therefore the solution is bounded.

Using the epidemiological feasible region, we want to verify that a transformation on the Zika virus will remain in a certain realistic limit for $t > 0$. Let $\Psi = \Omega_h + \Omega_v \subset R_+^1 \times R_+^2$ where

$$\Psi = \left\{(S_h, E_h, I_h, R_h, S_v, E_v, I_v) \in R_+^7 : N_h(t) \leq \frac{\Lambda_h}{\mu_h},\ N_v(t) \leq \left(\frac{\Lambda_v}{\mu_v}\right)\right\}.$$

Now, for positively invariant of R_+^7, from (12) we solve the inequalities as follows

$$N_h(t) \leq N_h(0)e^{-\mu_h(t)} + \frac{\Lambda_h}{\mu_h}\left(1 - e^{-\mu_h(t)}\right),\ N_v(t) \leq N_v(0)e^{-\mu_v(t)} + \frac{\Lambda_v}{\mu_v}\left(1 - e^{-\mu_v(t)}\right).$$

Therefore,

$$\limsup_{t\to\infty} N_h(t) \leq \frac{\Lambda_h}{\mu_h},\quad \limsup_{t\to\infty} N_v(t) \leq \frac{\Lambda_v}{\mu_v}.$$

Hence, the Zika virus transmission model is considered to be mathematically well posed, which means that all the solutions and initial conditions remains in the feasible region Ψ. □

Theorem 4.2. *The solution of (11) along with initial conditions is positively invariant and bounded in R_+^7.*

Proof. Using the results in [80] and taking the account of the initial values given, from model (11) we obtain

$$\begin{cases}
{}^{FABC}D_t^{\mu_*,\nu_*} S_h(t)|_{S_h=0} = \Lambda_h + \xi_h R_h > 0,\\
{}^{FABC}D_t^{\mu_*,\nu_*} E_h(t)|_{E_h=0} = (1-x_1)\lambda_h S_h > 0,\\
{}^{FABC}D_t^{\mu_*,\nu_*} I_h(t)|_{I_h=0} = \phi_h E_h > 0,\\
{}^{FABC}D_t^{\mu_*,\nu_*} R_h(t)|_{R_h=0} = \nu_h I_h > 0,\\
{}^{FABC}D_t^{\mu_*,\nu_*} S_v(t)|_{S_v=0} = \Lambda_v > 0,\\
{}^{FABC}D_t^{\mu_*,\nu_*} E_v(t)|_{E_v=0} = (1-x_1)\lambda_v S_v > 0,\\
{}^{FABC}D_t^{\mu_*,\nu_*} I_v(t)|_{I_v=0} = \phi_v E_v > 0.
\end{cases} \tag{13}$$

We know that $S_{h0} > 0, E_{h0} > 0, I_{h0} > 0, R_{h0} > 0, S_{v0} > 0, E_{v0} > 0, I_{v0} > 0$, for all $t > 0$. From (13), the result cannot escape from the hyperplanes. Consequently, the domain $\Psi = \{S_h(t), E_h(t), I_h(t),\ R_h(t), S_v(t), E_v(t), I_v(t)\} \in R_+^7$ is a positive invariant set. □

5. Existence and uniqueness

Before delving into any kind of epidemiological model or physical problem, it is significant to assess whether such a dynamical problem actually exists or does not exist. This concept can be derived by using various theories and tools. The Banach's fixed point technique help to answer this question. In this section, we use Banach's fixed point technique to analyse existence and uniqueness results of the fractal-fractional model (11). Consider the Banach space $\mathcal{M} = \mathbb{W}^7$ under the assumption that $\mathbb{W} = \mathcal{C}(\mathcal{J}, \mathbb{R})$ through the norm

$$\|\mathbf{D}\|_{\mathcal{M}} = \|\big(S_h, E_h, I_h, R_h, S_v, E_v, I_v\big)\|_{\mathcal{M}} = \sup\big\{|\mathcal{H}(t)| :\ \ t \in \mathcal{J}\big\},$$

such that $|\mathcal{H}| := |S_h| + |E_h| + |I_h| + |R_h| + |S_v| + |E_v| + |I_v|$. Similarly, the right-hand side of the fractal-fractional model (11) can be rewritten for simplicity as

$$\begin{aligned}
\mathbf{M}_1\big(t, S_h(t)\big) &= \Lambda_h + \xi_h R_h - (1-x_1)\lambda_h S_h - \mu_h S_h,\\
\mathbf{M}_2\big(t, E_h(t)\big) &= (1-x_1)\lambda_h S_h - \phi_h E_h - \mu_h E_h,\\
\mathbf{M}_3\big(t, I_h(t)\big) &= \phi_h E_h - (\nu_h + \eta_h) I_h - \mu_h I_h,\\
\mathbf{M}_4\big(t, R_h(t)\big) &= \nu_h I_h - \xi_h R_h - \mu_h R_h,\\
\mathbf{M}_5\big(t, S_v(t)\big) &= \Lambda_v - (1-x_1)\lambda_v S_v - \mu_v S_v,\\
\mathbf{M}_6\big(t, E_v(t)\big) &= (1-x_1)\lambda_v S_v - \phi_v E_v - \mu_v E_v,\\
\mathbf{M}_7\big(t, I_v(t)\big) &= \phi_v E_v - \mu_v I_v.
\end{aligned} \tag{14}$$

The fractal-fractional model (11) is reformulated as

$$\begin{cases} {}^{\mathbf{ABR}}\mathcal{D}_{0,t}^{\mu_*} S_h(t) = \nu_* t^{\nu_*-1}\mathbf{M}_1\big(t, S_h(t)\big), \\ {}^{\mathbf{ABR}}\mathcal{D}_{0,t}^{\mu_*} E_h(t) = \nu_* t^{\nu_*-1}\mathbf{M}_2\big(t, E_h(t)\big), \\ {}^{\mathbf{ABR}}\mathcal{D}_{0,t}^{\mu_*} I_h(t) = \nu_* t^{\nu_*-1}\mathbf{M}_3\big(t, I_h(t)\big), \\ {}^{\mathbf{ABR}}\mathcal{D}_{0,t}^{\mu_*} R_h(t) = \nu_* t^{\nu_*-1}\mathbf{M}_4\big(t, R_h(t)\big), \\ {}^{\mathbf{ABR}}\mathcal{D}_{0,t}^{\mu_*} S_v(t) = \nu_* t^{\nu_*-1}\mathbf{M}_5\big(t, S_v(t)\big), \\ {}^{\mathbf{ABR}}\mathcal{D}_{0,t}^{\mu_*} E_v(t) = \nu_* t^{\nu_*-1}\mathbf{M}_6\big(t, E_v(t)\big), \\ {}^{\mathbf{ABR}}\mathcal{D}_{0,t}^{\mu_*} I_v(t) = \nu_* t^{\nu_*-1}\mathbf{M}_7\big(t, I_v(t)\big). \end{cases} \tag{15}$$

Now, we consider the system (15), and reconstruct the extended mentioned system in the form of the compact initial value problem

$$\begin{cases} {}^{\mathbf{ABR}}\mathcal{D}_{0,t}^{\mu_*}\mathbf{D}(t) = \nu_* t^{\nu_*-1}\mathbf{M}\big(t, \mathbf{D}(t)\big), \\ \mathbf{D}(0) = \mathbf{D}_0, \end{cases} \tag{16}$$

with the assumption

$$\begin{aligned} \mathbf{D}(t) &= \big(S_h(t), E_h(t), I_h(t), R_h(t), S_v(t), E_v(t), I_v(t)\big)^T, \\ \mathbf{D}_0 &= \big(S_{h0}, E_{h0}, I_{h0}, R_{h0}, S_{v0}, E_{v0}, I_{v0}\big)^T, \quad \mu_*, \nu_* \in (0, 1], \end{aligned} \tag{17}$$

and

$$\mathbf{M}\big(t, \mathbf{D}(t)\big) = \begin{cases} \mathbf{M}_1\big(t, S_h(t)\big), \\ \mathbf{M}_2\big(t, E_h(t)\big), \\ \mathbf{M}_3\big(t, I_h(t)\big), \\ \mathbf{M}_4\big(t, R_h(t)\big), \\ \mathbf{M}_5\big(t, S_v(t)\big), \\ \mathbf{M}_6\big(t, E_v(t)\big), \\ \mathbf{M}_7\big(t, I_v(t)\big), \quad t \in \mathcal{J}. \end{cases} \tag{18}$$

Definition of the non-singular fractional ABR-derivative gives (16) as

$$\frac{\mathbf{G}(\mu_*)}{1-\mu_*}\frac{\mathrm{d}}{\mathrm{d}t}\int_0^t E_{\mu_*}\Big[-\frac{\mu_*}{1-\mu_*}(t-\mathfrak{s})^{\mu_*}\Big]\mathbf{D}(\mathfrak{s})\,\mathrm{d}\mathfrak{s} = \nu_* t^{\nu_*-1}\mathbf{M}\big(t, \mathbf{D}(t)\big). \tag{19}$$

Moreover, taking the fractal-fractional Atangana–Baleanu integral on (19), it yields

$$\begin{aligned} \mathbf{D}(t) = \mathbf{D}(0) &+ \frac{(1-\mu_*)\nu_* t^{\nu_*-1}}{\mathbf{G}(\mu_*)}\mathbf{M}(t, \mathbf{D}(t)) \\ &+ \frac{\mu_*\nu_*}{\Gamma(\mu_*)\mathbf{G}(\mu_*)}\int_0^t \mathfrak{s}^{\nu_*-1}(t-\mathfrak{s})^{\mu_*-1}\mathbf{M}(\mathfrak{s}, \mathbf{D}(\mathfrak{s}))\,\mathrm{d}\mathfrak{s}. \end{aligned} \tag{20}$$

By considering the above basic fractal-fractional integral equation, we obtain the following extended system of fractal-fractional integral equations as

$$\begin{aligned} S_h(t) &= S_{h0} + \frac{(1-\mu_*)\nu_* t^{\nu_*-1}}{\mathbf{G}(\mu_*)}\mathbf{M}_1(t, S_h(t)) \\ &\quad + \frac{\mu_*\nu_*}{\Gamma(\mu_*)\mathbf{G}(\mu_*)}\int_0^t \mathfrak{s}^{\nu_*-1}(t-\mathfrak{s})^{\mu_*-1}\mathbf{M}_1(\mathfrak{s}, S_h(\mathfrak{s}))\,\mathrm{d}\mathfrak{s}, \\ E_h(t) &= E_{h0} + \frac{(1-\mu_*)\nu_* t^{\nu_*-1}}{\mathbf{G}(\mu_*)}\mathbf{M}_2(t, E_h(t)) \\ &\quad + \frac{\mu_*\nu_*}{\Gamma(\mu_*)\mathbf{G}(\mu_*)}\int_0^t \mathfrak{s}^{\nu_*-1}(t-\mathfrak{s})^{\mu_*-1}\mathbf{M}_2(\mathfrak{s}, E_h(\mathfrak{s}))\,\mathrm{d}\mathfrak{s}, \\ I_h(t) &= I_{h0} + \frac{(1-\mu_*)\nu_* t^{\nu_*-1}}{\mathbf{G}(\mu_*)}\mathbf{M}_3(t, I_h(t)) \\ &\quad + \frac{\mu_*\nu_*}{\Gamma(\mu_*)\mathbf{G}(\mu_*)}\int_0^t \mathfrak{s}^{\nu_*-1}(t-\mathfrak{s})^{\mu_*-1}\mathbf{M}_3(\mathfrak{s}, I_h(\mathfrak{s}))\,\mathrm{d}\mathfrak{s}, \end{aligned}$$

$$
\begin{aligned}
R_h(t) &= R_{h0} + \frac{(1-\mu_*)\nu_* t^{\nu_*-1}}{\mathbf{G}(\mu_*)}\mathbf{M}_4(t, R_h(t)) \\
&\quad + \frac{\mu_*\nu_*}{\Gamma(\mu_*)\mathbf{G}(\mu_*)}\int_0^t \mathfrak{s}^{\nu_*-1}(t-\mathfrak{s})^{\mu_*-1}\mathbf{M}_4(\mathfrak{s}, R_h(\mathfrak{s}))\,\mathrm{d}\mathfrak{s}, \\
S_v(t) &= S_{v0} + \frac{(1-\mu_*)\nu_* t^{\nu_*-1}}{\mathbf{G}(\mu_*)}\mathbf{M}_5(t, S_v(t)) \\
&\quad + \frac{\mu_*\nu_*}{\Gamma(\mu_*)\mathbf{G}(\mu_*)}\int_0^t \mathfrak{s}^{\nu_*-1}(t-\mathfrak{s})^{\mu_*-1}\mathbf{M}_5(\mathfrak{s}, S_v(\mathfrak{s}))\,\mathrm{d}\mathfrak{s}, \\
E_v(t) &= E_{v0} + \frac{(1-\mu_*)\nu_* t^{\nu_*-1}}{\mathbf{G}(\mu_*)}\mathbf{M}_6(t, E_v(t)) \\
&\quad + \frac{\mu_*\nu_*}{\Gamma(\mu_*)\mathbf{G}(\mu_*)}\int_0^t \mathfrak{s}^{\nu_*-1}(t-\mathfrak{s})^{\mu_*-1}\mathbf{M}_6(\mathfrak{s}, E_v(\mathfrak{s}))\,\mathrm{d}\mathfrak{s}, \\
I_v(t) &= I_{v0} + \frac{(1-\mu_*)\nu_* t^{\nu_*-1}}{\mathbf{G}(\mu_*)}\mathbf{M}_7(t, I_v(t)) \\
&\quad + \frac{\mu_*\nu_*}{\Gamma(\mu_*)\mathbf{G}(\mu_*)}\int_0^t \mathfrak{s}^{\nu_*-1}(t-\mathfrak{s})^{\mu_*-1}\mathbf{M}_7(\mathfrak{s}, I_v(\mathfrak{s}))\,\mathrm{d}\mathfrak{s}.
\end{aligned}
$$

We regard a new map to investigate a fixed-point problem, by giving $T : \mathcal{M} \to \mathcal{M}$ as

$$
\begin{aligned}
T(\mathbf{D}(t)) &= \mathbf{D}(0) + \frac{(1-\mu_*)\nu_* t^{\nu_*-1}}{\mathbf{G}(\mu_*)}\mathbf{M}(t, \mathbf{D}(t)) \\
&\quad + \frac{\mu_*\nu_*}{\Gamma(\mu_*)\mathbf{G}(\mu_*)}\int_0^t \mathfrak{s}^{\nu_*-1}(t-\mathfrak{s})^{\mu_*-1}\mathbf{M}(\mathfrak{s}, \mathbf{D}(\mathfrak{s}))\,\mathrm{d}\mathfrak{s}.
\end{aligned} \tag{21}
$$

In relation to the existence property of solution on the Zika fractal-fractional model (11), the following is deploy:

Theorem 5.1 (*[81] Leray–Schauder Theorem*)**.** *Let $\mathcal{M}$ be a Banach space, $U \subset \mathcal{M}$ a convex closed bounded set, $\mathbb{G} \subset U$ an open set, and $0 \in \mathbb{G}$. Then for the continuous and compact map $T : \bar{\mathbb{G}} \to U$, either:*

(HY1) $\exists\, m \in \bar{\mathbb{G}}\, s.t.\, m = T(m)$, *or*
(HY2) $\exists\, m \in \partial\mathbb{G}$ *and* $0 < \mu < 1$ *s.t.* $m = \mu T(m)$.

Theorem 5.2. *Let $\mathbf{M} \in \mathcal{C}(\mathcal{J} \times \mathcal{M}, \mathcal{M})$, and also assume:*

(G1) $\exists\, \mathcal{F} \in L^1(\mathcal{J}, \mathbb{R}^+)$ *and* $\exists\, \Upsilon \in C([0,\infty), (0,\infty))$ *(Υ is non-decreasing) s.t.* $\forall\, t \in \mathcal{J}$ *and* $\mathbf{D} \in \mathcal{M}$,

$$\left|\mathbf{M}(t, \mathbf{D}(t))\right| \le \mathcal{F}(t)\Upsilon(|\mathbf{D}(t)|);$$

(G2) $\exists\, \mathfrak{R}^* > 0$ *s.t.*

$$\frac{\mathfrak{R}^*}{\left[\frac{(1-\mu_*)\nu_*\tau^{\nu_*-1}}{\mathbf{G}(\mu_*)} + \frac{\mu_*\nu_*\tau^{\mu_*+\nu_*-1}\Gamma(\nu_*)}{\Gamma(\mu_*+\nu_*)\mathbf{G}(\mu_*)}\right]\mathcal{F}_0^*\Upsilon(\mathfrak{R}^*) + \mathbf{D}_0} > 1, \tag{22}$$

with $\mathcal{F}_0^* = \sup_{t\in\mathcal{J}} |\mathcal{F}(t)|$.

Then for the fractal-fractional problem (16) and so, for the fractal-fractional model (11), at least a solution exists on $\mathcal{J}$.

Proof. To start our argument, consider $T : \mathcal{M} \to \mathcal{M}$ given by (21) and

$$N_{R^*} = \left\{\mathbf{D} \in \mathcal{M} \,:\, \|\mathbf{D}\|_{\mathcal{M}} \le R^*\right\}, \quad \text{for some } R^* > 0.$$

Evidently, the continuity of $\mathbf{M}$ implies that of the operator T. Now (G1) gives the following estimate

$$
\begin{aligned}
\left|T(\mathbf{D}(t))\right| &\le \left|\mathbf{D}(0)\right| + \frac{(1-\mu_*)\nu_* t^{\nu_*-1}}{\mathbf{G}(\mu_*)}\left|\mathbf{M}(t, \mathbf{D}(t))\right| \\
&\quad + \frac{\mu_*\nu_*}{\Gamma(\mu_*)\mathbf{G}(\mu_*)}\int_0^t \mathfrak{s}^{\nu_*-1}(t-\mathfrak{s})^{\mu_*-1}\left|\mathbf{M}(\mathfrak{s}, \mathbf{D}(\mathfrak{s}))\right|\mathrm{d}\mathfrak{s} \\
&\le \mathbf{D}_0 + \frac{(1-\mu_*)\nu_* t^{\nu_*-1}}{\mathbf{G}(\mu_*)}\mathcal{F}(t)\Upsilon(|\mathbf{D}(t)|) \\
&\quad + \frac{\mu_*\nu_*}{\Gamma(\mu_*)\mathbf{G}(\mu_*)}\int_0^t \mathfrak{s}^{\nu_*-1}(t-\mathfrak{s})^{\mu_*-1}\mathcal{F}(\mathfrak{s})\Upsilon(|\mathbf{D}(\mathfrak{s})|)\,\mathrm{d}\mathfrak{s}
\end{aligned}
$$

$$\leq \mathbf{D}_0 + \frac{(1-\mu_*)\nu_*\tau^{\nu_*-1}}{\mathbf{G}(\mu_*)}\mathcal{F}_0^*\Upsilon(R^*) + \frac{\mu_*\nu_*\tau^{\mu_*+\nu_*-1}B(\mu_*,\nu_*)}{\Gamma(\mu_*)\mathbf{G}(\mu_*)}\mathcal{F}_0^*\Upsilon(R^*)$$
$$= \mathbf{D}_0 + \frac{(1-\mu_*)\nu_*\tau^{\nu_*-1}}{\mathbf{G}(\mu_*)}\mathcal{F}_0^*\Upsilon(R^*) + \frac{\mu_*\nu_*\tau^{\mu_*+\nu_*-1}\Gamma(\nu_*)}{\mathbf{G}(\mu_*)\Gamma(\mu_*+\nu_*)}\mathcal{F}_0^*\Upsilon(R^*),$$

for $\mathbf{D} \in N_{R^*}$. We get

$$\|T\mathbf{D}\|_{\mathbb{M}} \leq \mathbf{D}_0 + \Big[\frac{(1-\mu_*)\nu_*\tau^{\nu_*-1}}{\mathbf{G}(\mu_*)} + \frac{\mu_*\nu_*\tau^{\mu_*+\nu_*-1}\Gamma(\nu_*)}{\mathbf{G}(\mu_*)\Gamma(\mu_*+\nu_*)}\Big]\mathcal{F}_0^*\Upsilon(R^*) < \infty. \tag{23}$$

So $\|T\mathbf{D}\|_{\mathbb{M}} < \infty$ and T is uniformly bounded on $\mathcal{M}$. In the following, choose $t, z \in [0,\tau] := \mathcal{J}$ arbitrarily with $t < z$ and $\mathbf{D} \in N_{R^*}$. Take

$$\sup_{(t,\mathbf{D})\in\mathcal{J}\times N_{R^*}} |\mathbf{M}(t,\mathbf{D}(t))| = \mathbf{M}^* < \infty.$$

Then

$$\begin{aligned}
\big|T(\mathbf{D}(z)) - T(\mathbf{D}(t))\big| &\leq \Big|\frac{(1-\mu_*)\nu_* z^{\nu_*-1}}{\mathbf{G}(\mu_*)}\mathbf{M}(z,\mathbf{D}(z)) - \frac{(1-\mu_*)\nu_* t^{\nu_*-1}}{\mathbf{G}(\mu_*)}\mathbf{M}(t,\mathbf{D}(t))\\
&+ \frac{\mu_*\nu_*}{\Gamma(\mu_*)\mathbf{G}(\mu_*)}\int_0^z \mathfrak{s}^{\nu_*-1}(z-\mathfrak{s})^{\mu_*-1}\mathbf{M}(\mathfrak{s},\mathbf{D}(\mathfrak{s}))\,\mathrm{d}\mathfrak{s}\\
&- \frac{\mu_*\nu_*}{\Gamma(\mu_*)\mathbf{G}(\mu_*)}\int_0^t \mathfrak{s}^{\nu_*-1}(t-\mathfrak{s})^{\mu_*-1}\mathbf{M}(\mathfrak{s},\mathbf{D}(\mathfrak{s}))\,\mathrm{d}\mathfrak{s}\Big|\\
&\leq \frac{(1-\mu_*)\nu_*\mathbf{M}^*}{\mathbf{G}(\mu_*)}(z^{\nu_*-1} - t^{\nu_*-1})\\
&+ \frac{\mu_*\nu_*\mathbf{M}^*}{\Gamma(\mu_*)\mathbf{G}(\mu_*)}\Big|\int_0^z \mathfrak{s}^{\nu_*-1}(z-\mathfrak{s})^{\mu_*-1}\,\mathrm{d}\mathfrak{s} - \int_0^t \mathfrak{s}^{\nu_*-1}(t-\mathfrak{s})^{\mu_*-1}\,\mathrm{d}\mathfrak{s}\Big|\\
&\leq \frac{(1-\mu_*)\nu_*\mathbf{M}^*}{\mathbf{G}(\mu_*)}(z^{\nu_*-1} - t^{\nu_*-1}) + \frac{\mu_*\nu_*\mathbf{M}^*B(\mu_*,\nu_*)}{\Gamma(\mu_*)\mathbf{G}(\mu_*)}\big[z^{\mu_*+\nu_*-1} - t^{\mu_*+\nu_*-1}\big]\\
&= \frac{(1-\mu_*)\nu_*\mathbf{M}^*}{\mathbf{G}(\mu_*)}(z^{\nu_*-1} - t^{\nu_*-1}) + \frac{\mu_*\nu_*\mathbf{M}^*\Gamma(\nu_*)}{\Gamma(\mu_*+\nu_*)\mathbf{G}(\mu_*)}\big[z^{\mu_*+\nu_*-1} - t^{\mu_*+\nu_*-1}\big],
\end{aligned} \tag{24}$$

where (independent of $\mathbf{D}$) (24) tends to 0 as $z \to t$. Therefore,

$$\lim_{z\to t}\|T(\mathbf{D}(z)) - T(\mathbf{D}(t))\|_{\mathcal{M}} = 0,$$

and T is equicontinuous, and so it is compact on N_{R^*} by referring to the Arzelá–Ascoli theorem. Since all the conditions of Theorem 5.1 to be held on T, thus one of (HY1) or (HY2) will be valid. From (G2), set

$$\Phi := \Big\{\mathbf{D} \in \mathcal{M} : \ \|\mathbf{D}\|_{\mathcal{M}} < \mathfrak{R}^*\Big\},$$

for some $\mathfrak{R}^* > 0$ via $\mathbf{D}_0 + \Big[\frac{(1-\mu_*)\nu_*\tau^{\nu_*-1}}{\mathbf{G}(\mu_*)} + \frac{\mu_*\nu_*\tau^{\mu_*+\nu_*-1}\Gamma(\nu_*)}{\Gamma(\mu_*+\nu_*)\mathbf{G}(\mu_*)}\Big]\mathcal{F}_0^*\Upsilon(\mathfrak{R}^*) < \mathfrak{R}^*$. With the help of (G1) and by (23), we estimate

$$\|T\mathbf{D}\|_{\mathcal{M}} \leq \mathbf{D}_0 + \Big[\frac{(1-\mu_*)\nu_*\tau^{\nu_*-1}}{\mathbf{G}(\mu_*)} + \frac{\mu_*\nu_*\tau^{\mu_*+\nu_*-1}\Gamma(\nu_*)}{\Gamma(\mu_*+\nu_*)\mathbf{G}(\mu_*)}\Big]\mathcal{F}_0^*\Upsilon(\|\mathbf{D}\|_{\mathcal{M}}). \tag{25}$$

Next, we consider the existence of $\mathbf{D} \in \partial\Phi$ and $0 < \mu < 1$ with $\mathbf{D} = \mu T(\mathbf{D})$. For these selections of $\mathbf{D}$ and μ, and by (25),

$$\begin{aligned}
\mathfrak{R}^* = \|\mathbf{D}\|_{\mathcal{M}} = \mu\|T\mathbf{D}\|_{\mathcal{M}} &< \mathbf{D}_0 + \Big[\frac{(1-\mu_*)\nu_*\tau^{\nu_*-1}}{\mathbf{G}(\mu_*)} + \frac{\mu_*\nu_*\tau^{\mu_*+\nu_*-1}\Gamma(\nu_*)}{\Gamma(\mu_*+\nu_*)\mathbf{G}(\mu_*)}\Big]\mathcal{F}_0^*\Upsilon(\|\mathbf{D}\|_{\mathcal{M}})\\
&< \mathbf{D}_0 + \Big[\frac{(1-\mu_*)\nu_*\tau^{\nu_*-1}}{\mathbf{G}(\mu_*)} + \frac{\mu_*\nu_*\tau^{\mu_*+\nu_*-1}\Gamma(\nu_*)}{\Gamma(\mu_*+\nu_*)\mathbf{G}(\mu_*)}\Big]\mathcal{F}_0^*\Upsilon(\mathfrak{R}^*) < \mathfrak{R}^*,
\end{aligned}$$

which is unachievable. Therefore, (HY2) does not satisfy and T possesses a fixed-point in $\bar{\Phi}$ by Theorem 5.1 which is the same solution of the fractal-fractional model (11). □

To demonstrate the uniqueness of the fractal-fractional model (11), we examine the Lipschitz property for the kernels $\mathbf{M}_\jmath$, $(\jmath = 1,\ldots,7)$ examined in (14).

Lemma 5.3. *Let $S_h, E_h, I_h, R_h, S_v, E_v, I_v, S_h^*, E_h^*, I_h^*, R_h^*, S_v^*, E_v^*, I_v^* \in \mathbb{W} := \mathcal{C}(\mathcal{J},\mathbb{R})$, and for all $t \in \mathcal{J}$, $1+\varphi_2 I_h^*(t) > I_h(t)$, $1+\varphi_2 I_v^*(t) > I_v(t)$, and*

*(**V**3) $\exists\, \varkappa_1^*, \varkappa_2^*, \varkappa_3^*, \varkappa_4^*, \varkappa_5^*, \varkappa_6^*, \varkappa_7^* > 0$ s.t. $\|S_h\| \leq \varkappa_1^*$, $\|E_h\| \leq \varkappa_2^*$, $\|I_h\| \leq \varkappa_3^*$, $\|R_h\| \leq \varkappa_4^*$, $\|S_v\| \leq \varkappa_5^*$, $\|E_v\| \leq \varkappa_6^*$ and $\|I_v\| \leq \varkappa_7^*$.*

Then $\mathbf{M}_1, \mathbf{M}_2, \mathbf{M}_3, \mathbf{M}_4, \mathbf{M}_5, \mathbf{M}_6, \mathbf{M}_7$ *defined by* (14) *are Lipschitz with* $\mathbf{L}_1^*, \mathbf{L}_2^*, \mathbf{L}_3^*, \mathbf{L}_4^*, \mathbf{L}_5^*, \mathbf{L}_6^*, \mathbf{L}_7^* > 0$, *where*

$$\begin{aligned} &\mathbf{L}_1^* = (1-x_1)\lambda_h + \mu_h > 0,\ \mathbf{L}_2^* = \phi_h + \mu_h > 0,\ \mathbf{L}_3^* = (\nu_h + \eta_h) + \mu_h > 0, \\ &\mathbf{L}_4^* = \xi_h + \mu_h > 0,\ \mathbf{L}_5^* = (1-x_1)\lambda_v + \mu_v > 0,\ \mathbf{L}_6^* = \phi_v + \mu_v > 0,\ \mathbf{L}_7^* = \mu_v > 0. \end{aligned} \tag{26}$$

Proof. For $\mathbf{M}_1$, we select $S_h, S_h^* \in \mathbb{W} := \mathcal{C}(\mathcal{J}, \mathbb{R})$ at random. Then

$$\begin{aligned} &\|\mathbf{M}_1(t, S_h(t)) - \mathbf{M}_1(t, S_h^*(t))\| \\ &\quad = \Big\| \Big[\Lambda_h + \xi_h R_h - (1-x_1)\lambda_h S_h - \mu_h S_h \Big] \\ &\quad - \Big[\Lambda_h + \xi_h R_h - (1-x_1)\lambda_h S_h^* - \mu_h S_h^* \Big] \Big\| \\ &\quad \le \Big\| \Big[(1-x_1)\lambda_h + \mu_h \Big] \big(S_h(t) - S_h^*(t) \big) \Big\| \\ &\quad = \mathbf{L}_1^* \| S_h(t) - S_h^*(t) \|. \end{aligned}$$

This indicates that $\mathbf{M}_1$ is Lipschitz w.r.t. S_h with constant $\mathbf{L}_1^* > 0$. For the function $\mathbf{M}_2$, we select $E_h, E_h^* \in \mathbb{W} := \mathcal{C}(\mathcal{J}, \mathbb{R})$ at random. Then

$$\begin{aligned} &\|\mathbf{M}_2(t, E_h(t)) - \mathbf{M}_2(t, E_h^*(t))\| \\ &\quad = \Big\| \Big[(1-x_1)\lambda_h S_h - \phi_h E_h - \mu_h E_h \Big] \\ &\quad - \Big[(1-x_1)\lambda_h S_h - \phi_h E_h^* - \mu_h E_h^* \Big] \Big\| \\ &\quad \le \big[\phi_h + \mu_h \big] \| E_h(t) - E_h^*(t) \| \\ &\quad = \mathbf{L}_2^* \| E_h(t) - E_h^*(t) \|. \end{aligned}$$

This indicates that $\mathbf{M}_2$ is Lipschitz w.r.t. E_h with constant $\mathbf{L}_2^* > 0$. For $\mathbf{M}_3$, we select $I_h, I_h^* \in \mathbb{W} := \mathcal{C}(\mathcal{J}, \mathbb{R})$ at random. Then

$$\begin{aligned} &\|\mathbf{M}_3(t, I_h(t)) - \mathbf{M}_3(t, I_h^*(t))\| \\ &\quad = \Big\| \Big[\phi_h E_h - (\nu_h + \eta_h) I_h - \mu_h I_h \Big] \\ &\quad - \Big[\phi_h E_h - (\nu_h + \eta_h) I_h^* - \mu_h I_h^* \Big] \Big\| \\ &\quad \le \big[(\nu_h + \eta_h) + \mu_h \big] \| I_h(t) - I_h^*(t) \| \\ &\quad = \mathbf{L}_3^* \| I_h(t) - I_h^*(t) \|. \end{aligned}$$

This indicates that $\mathbf{M}_3$ is Lipschitz w.r.t. I_h with constant $\mathbf{L}_3^* > 0$. For $\mathbf{M}_4$, we select $R_h, R_h^* \in \mathbb{W} := \mathcal{C}(\mathcal{J}, \mathbb{R})$ at random. Then

$$\begin{aligned} &\|\mathbf{M}_4(t, R_h(t)) - \mathbf{M}_4(t, R_h^*(t))\| \\ &\quad = \Big\| \Big[\nu_h I_h - \xi_h R_h - \mu_h R_h \Big] \\ &\quad - \Big[\nu_h I_h - \xi_h R_h^* - \mu_h R_h^* \Big] \Big\| \\ &\quad \le \big[\xi_h + \mu_h \big] \| R_h(t) - R_h^*(t) \| \\ &\quad = \mathbf{L}_4^* \| R_h(t) - R_h^*(t) \|. \end{aligned}$$

This indicates that $\mathbf{M}_4$ is Lipschitz w.r.t. R_h with constant $\mathbf{L}_4^* > 0$. For $\mathbf{M}_5$, we select $S_v, S_v^* \in \mathbb{W} := \mathcal{C}(\mathcal{J}, \mathbb{R})$ at random. Then

$$\begin{aligned} &\|\mathbf{M}_5(t, S_v(t)) - \mathbf{M}_5(t, S_v^*(t))\| \\ &\quad = \Big\| \Big[\Lambda_v - (1-x_1)\lambda_v S_v - \mu_v S_v \Big] \\ &\quad - \Big[\Lambda_v - (1-x_1)\lambda_v S_v^* - \mu_v S_v^* \Big] \Big\| \\ &\quad \le \big[(1-x_1) + \mu_v \big] \| S_v(t) - S_v^*(t) \| \\ &\quad = \mathbf{L}_5^* \| S_v(t) - S_v^*(t) \|. \end{aligned}$$

This indicates that $\mathbf{M}_5$ is Lipschitz w.r.t. S_v with constant $\mathbf{L}_5^* > 0$. For $\mathbf{M}_6$, we select $E_v, E_v^* \in \mathbb{W} := \mathcal{C}(\mathcal{J}, \mathbb{R})$ at random. Then

$$\begin{aligned} &\|\mathbf{M}_6(t, E_v(t)) - \mathbf{M}_6(t, E_v^*(t))\| \\ &\quad = \Big\| \Big[(1-x_1)\lambda_v S_v - \phi_v E_v - \mu_v E_v \Big] \end{aligned}$$

$$
\begin{aligned}
&- \Big[(1-x_1)\lambda_v S_v - \phi_v E_v^* - \mu_v E_v^*\Big]\Big\| \\
&\leq \big[\phi_v + \mu_v\big]\|E_v(t) - E_v^*(t)\| \\
&= \mathbf{L}_6^*\|E_v(t) - E_v^*(t)\|.
\end{aligned}
$$

This indicates that $\mathbf{M}_6$ is Lipschitz w.r.t. S_v with constant $\mathbf{L}_6^* > 0$. Finally, for $\mathbf{M}_7$, we select $I_v, I_v{}^* \in \mathbb{W} := \mathcal{C}(\mathcal{J}, \mathbb{R})$ at random. Then

$$
\begin{aligned}
&\|\mathbf{M}_7\big(t, I_v(t)\big) - \mathbf{M}_7\big(t, I_v{}^*(t)\big)\| \\
&\qquad = \Big\|\Big[\phi_v E_v - \mu_v I_v\Big] \\
&\qquad - \Big[\phi_v E_v - \mu_v I_v^*\Big]\Big\| \\
&\qquad \leq \mu_v\|I_v(t) - I_v{}^*(t)\| \\
&\qquad = \mathbf{L}_7^*\|I_v(t) - I_v{}^*(t)\|.
\end{aligned}
$$

This indicates that $\mathbf{M}_7$ is Lipschitz w.r.t. I_v with constant $\mathbf{L}_7^* > 0$. The proof for all given $\mathcal{M}_j, j = 1\cdots 7$ functions is completed. □

Theorem 5.4. *Let (**V**3) be fixed. Then the fractal-fractional model (11) has a unique solution when*

$$
\Big[\frac{(1-\mu_*)\nu_*\tau^{\nu_*-1}}{\mathbf{G}(\mu_*)} + \frac{\mu_*\nu_*\Gamma(\nu_*)\tau^{\mu_*+\nu_*-1}}{\Gamma(\mu_*+\nu_*)\mathbf{G}(\mu_*)}\Big]\mathbf{L}_j^* < 1, \quad (j \in \{1,\ldots,7\}), \tag{27}
$$

and $\mathbf{L}_j^*$'s are introduced in (26).

Proof. We presume that the theorem's conclusion is invalid. Consequently, alternative solution is possible for the fractal-fractional model (11). Consider the expression $\big(S_h^*, E_h^*, I_h^*, R_h^*, S_v^*, E_v^*, I_v^*\big)$ is another solution under the initial value condition

$$
\big(S_h^*(0), E_h^*(0), I_h^*(0), R_h^*(0), S_v^*(0), E_v^*(0), I_v{}^*(0)\big) = \big(S_{h0}, I_{h0}, I_{h0}, R_{h0}, S_{v0}, E_{v0}, I_v\big).
$$

Then by (20), we have

$$
\begin{aligned}
S_h^*(t) &= S_{h0} + \frac{(1-\mu_*)\nu_* t^{\nu_*-1}}{\mathbf{G}(\mu_*)}\mathbf{M}_1(t, S_h^*(t)) \\
&\quad + \frac{\mu_*\nu_*}{\Gamma(\mu_*)\mathbf{G}(\mu_*)}\int_0^t \mathfrak{s}^{\nu_*-1}(t-\mathfrak{s})^{\mu_*-1}\mathbf{M}_1(\mathfrak{s}, S_h^*(\mathfrak{s}))\,d\mathfrak{s}, \\
E_h^*(t) &= E_{h0} + \frac{(1-\mu_*)\nu_* t^{\nu_*-1}}{\mathbf{G}(\mu_*)}\mathbf{M}_2(t, E_h^*(t)) \\
&\quad + \frac{\mu_*\nu_*}{\Gamma(\mu_*)\mathbf{G}(\mu_*)}\int_0^t \mathfrak{s}^{\nu_*-1}(t-\mathfrak{s})^{\mu_*-1}\mathbf{M}_2(\mathfrak{s}, E_h^*(\mathfrak{s}))\,d\mathfrak{s}, \\
I_h^*(t) &= I_{h0}^h + \frac{(1-\mu_*)\nu_* t^{\nu_*-1}}{\mathbf{G}(\mu_*)}\mathbf{M}_3(t, I_h^*(t)) \\
&\quad + \frac{\mu_*\nu_*}{\Gamma(\mu_*)\mathbf{G}(\mu_*)}\int_0^t \mathfrak{s}^{\nu_*-1}(t-\mathfrak{s})^{\mu_*-1}\mathbf{M}_3(\mathfrak{s}, I_h^*(\mathfrak{s}))\,d\mathfrak{s}, \\
R_h^*(t) &= R_{h0} + \frac{(1-\mu_*)\nu_* t^{\nu_*-1}}{\mathbf{G}(\mu_*)}\mathbf{M}_4(t, R_h^*(t)) \\
&\quad + \frac{\mu_*\nu_*}{\Gamma(\mu_*)\mathbf{G}(\mu_*)}\int_0^t \mathfrak{s}^{\nu_*-1}(t-\mathfrak{s})^{\mu_*-1}\mathbf{M}_4(\mathfrak{s}, R_h^*(\mathfrak{s}))\,d\mathfrak{s}, \\
S_v^*(t) &= S_{v0} + \frac{(1-\mu_*)\nu_* t^{\nu_*-1}}{\mathbf{G}(\mu_*)}\mathbf{M}_5(t, S_v^*(t)) \\
&\quad + \frac{\mu_*\nu_*}{\Gamma(\mu_*)\mathbf{G}(\mu_*)}\int_0^t \mathfrak{s}^{\nu_*-1}(t-\mathfrak{s})^{\mu_*-1}\mathbf{M}_5(\mathfrak{s}, S_v^*(\mathfrak{s}))\,d\mathfrak{s}, \\
E_v^*(t) &= E_{v0} + \frac{(1-\mu_*)\nu_* t^{\nu_*-1}}{\mathbf{G}(\mu_*)}\mathbf{M}_6(t, E_v^*(t)) \\
&\quad + \frac{\mu_*\nu_*}{\Gamma(\mu_*)\mathbf{G}(\mu_*)}\int_0^t \mathfrak{s}^{\nu_*-1}(t-\mathfrak{s})^{\mu_*-1}\mathbf{M}_6(\mathfrak{s}, E_v^*(\mathfrak{s}))\,d\mathfrak{s},
\end{aligned}
$$

$$I_v{}^*(t) = I_{v0}^v + \frac{(1-\mu_*)\nu_* t^{\nu_*-1}}{\mathbf{G}(\mu_*)}\mathbf{M}_7(t, I_v{}^*(t)) + \frac{\mu_*\nu_*}{\Gamma(\mu_*)\mathbf{G}(\mu_*)}\int_0^t \mathfrak{s}^{\nu_*-1}(t-\mathfrak{s})^{\mu_*-1}\mathbf{M}_7(\mathfrak{s}, I_v{}^*(\mathfrak{s}))\,\mathrm{d}\mathfrak{s}.$$

Therefore, we can now estimate

$$\begin{aligned}|S_h(t) - S_h^*(t)| &\le \frac{(1-\mu_*)\nu_* t^{\nu_*-1}}{\mathbf{G}(\mu_*)}\Big|\mathbf{M}_1(t, S_h(t)) - \mathbf{M}_1(t, S_h^*(t))\Big| \\ &+ \frac{\mu_*\nu_*}{\Gamma(\mu_*)\mathbf{G}(\mu_*)}\int_0^t \mathfrak{s}^{\nu_*-1}(t-\mathfrak{s})^{\mu_*-1}\Big|\mathbf{M}_1(\mathfrak{w}^*, S_h(\mathfrak{w}^*)) - \mathbf{M}_1(\mathfrak{w}^*, S_h^*(\mathfrak{w}^*))\Big|\,\mathrm{d}\mathfrak{w}^* \\ &\le \frac{(1-\mu_*)\nu_* t^{\nu_*-1}}{\mathbf{G}(\mu_*)}\mathbf{L}_1^*\|S_h - S_h^*\| + \frac{\mu_*\nu_*}{\Gamma(\mu_*)\mathbf{G}(\mu_*)}\int_0^t \mathfrak{s}^{\nu_*-1}(t-\mathfrak{s})^{\mu_*-1}\mathbf{L}_1^*\|S_h - S_h^*\|\,\mathrm{d}\mathfrak{w}^* \\ &\le \Big[\frac{(1-\mu_*)\nu_*\tau^{\nu_*-1}}{\mathbf{G}(\mu_*)} + \frac{\mu_*\nu_*\Gamma(\nu_*)\tau^{\mu_*+\nu_*-1}}{\Gamma(\mu_*+\nu_*)\mathbf{G}(\mu_*)}\Big]\mathbf{L}_1^*\|S_h - S_h^*\|,\end{aligned}$$

hence

$$\left(1 - \Big[\frac{(1-\mu_*)\nu_*\tau^{\nu_*-1}}{\mathbf{G}(\mu_*)} + \frac{\mu_*\nu_*\Gamma(\nu_*)\tau^{\mu_*+\nu_*-1}}{\Gamma(\mu_*+\nu_*)\mathbf{G}(\mu_*)}\Big]\mathbf{L}_1^*\right)\|S_h - S_h^*\| \le 0.$$

The above inequality holds when $\|S_h - S_h^*\| = 0$, or $S_h = S_h^*$. In the similar manner, from the inequality

$$\|E_h - E_h^*\| \le \Big[\frac{(1-\mu_*)\nu_*\tau^{\nu_*-1}}{\mathbf{G}(\mu_*)} + \frac{\mu_*\nu_*\Gamma(\nu_*)\tau^{\mu_*+\nu_*-1}}{\Gamma(\mu_*+\nu_*)\mathbf{G}(\mu_*)}\Big]\mathbf{L}_2^*\|E_h - E_h^*\|,$$

we now arrive at

$$\left(1 - \Big[\frac{(1-\mu_*)\nu_*\tau^{\nu_*-1}}{\mathbf{G}(\mu_*)} + \frac{\mu_*\nu_*\Gamma(\nu_*)\tau^{\mu_*+\nu_*-1}}{\Gamma(\mu_*+\nu_*)\mathbf{G}(\mu_*)}\Big]\mathbf{L}_2^*\right)\|E_h - E_h^*\| \le 0.$$

This is valid when $\|E_h - E_h^*\| = 0$ or $E_h = E_h^*$. Furthermore, the inequality

$$\|I_h - I_h^*\| \le \Big[\frac{(1-\mu_*)\nu_*\tau^{\nu_*-1}}{\mathbf{G}(\mu_*)} + \frac{\mu_*\nu_*\Gamma(\nu_*)\tau^{\mu_*+\nu_*-1}}{\Gamma(\mu_*+\nu_*)\mathbf{G}(\mu_*)}\Big]\mathbf{L}_3^*\|I_h - I_h^*\|,$$

which gives

$$\left(1 - \Big[\frac{(1-\mu_*)\nu_*\tau^{\nu_*-1}}{\mathbf{G}(\mu_*)} + \frac{\mu_*\nu_*\Gamma(\nu_*)\tau^{\mu_*+\nu_*-1}}{\Gamma(\mu_*+\nu_*)\mathbf{G}(\mu_*)}\Big]\mathbf{L}_3^*\right)\|I_h - I_h^*\| \le 0.$$

This is valid when $\|I_h - I_h^*\| = 0$ or $I_h = I_h^*$. In similar manner, we can ascertain that get $R_h = R_h^*$, $S_v = S_v^*$, $E_v = E_v^*$ and $I_v = I_v{}^*$. Therefore, for each $t \in \mathcal{J}$, we get

$$\big(S_h(t), E_h(t), I_h(t), R_h(t), S_v(t), E_v(t), I_v(t)\big) = \big(S_h^*(t), E_h^*(t), I_h^*(t), R_h^*(t), S_v^*(t), E_v^*(t), I_v^*(t)\big).$$

Hence the fractal-fractional model (11) has a unique solution if (27) holds. □

6. Hyers-Ulam stability (HU)

Stability plays a significant role as far as the differential equation is concern. Among the several types of stability, HU type stability is one of the most intriguing, recently. The HU stability was first introduced by [82] and later generalized in the paper published by Rassias [83]. This stability-type is useful in a variety of natural phenomena where searching for the exact or precise solution is complicated. In epidemiological model, where sometimes is quite difficult to get exact solution, HU stability is use to get approximate solution to control the dynamism of the virus. For this purpose, in this analysis, due to complication in transmission dynamism of Zika virus, we apply HU stability concept to study stability nature of the fractal-fractional model (11).

Definition 6.1. The fractal-fractional model (11) is UH-stable if $\exists\, 0 < \mathcal{Q}_{\mathbf{M}_J} \in \mathbb{N}$, $J \in \{1, \ldots, 7\}$ s.t. $\forall\, \mathbb{N}_J > 0$, and $\forall \left(S_h^*, E_h^*, I_h^*, R_h^*, S_v^*, E_v^*, I_v^*\right) \in \mathcal{M}$ satisfying

$$\begin{aligned}&\Big|{}^{\mathbf{FFML}}\mathcal{D}_{0,t}^{(\mu_*,\nu_*)}S_h^*(t) - \mathbf{M}_1\big(t, S_h^*(t)\big)\Big| < \mathbb{N}_1, \\ &\Big|{}^{\mathbf{FFML}}\mathcal{D}_{0,t}^{(\mu_*,\nu_*)}E_h^*(t) - \mathbf{M}_2\big(t, E_v^*(t)\big)\Big| < \mathbb{N}_2, \\ &\Big|{}^{\mathbf{FFML}}\mathcal{D}_{0,t}^{(\mu_*,\nu_*)}I_h^*(t) - \mathbf{M}_3\big(t, I_h^*(t)\big)\Big| < \mathbb{N}_3,\end{aligned}$$

$$\begin{aligned}
&\left|{}^{\mathbf{FFML}}\mathcal{D}_{0,t}^{(\mu_*,\nu_*)}R_h^*(t)-\mathbf{M}_4\big(t,R_h^*(t)\big)\right|<\mathbb{N}_4,\\
&\left|{}^{\mathbf{FFML}}\mathcal{D}_{0,t}^{(\mu_*,\nu_*)}S_v^*(t)-\mathbf{M}_5\big(t,S_v^*(t)\big)\right|<\mathbb{N}_5,\\
&\left|{}^{\mathbf{FFML}}\mathcal{D}_{0,t}^{(\mu_*,\nu_*)}E_v^*(t)-\mathbf{M}_6\big(t,E_v^*(t)\big)\right|<\mathbb{N}_6,\\
&\left|{}^{\mathbf{FFML}}\mathcal{D}_{0,t}^{(\mu_*,\nu_*)}I_v^*(t)-\mathbf{M}_7\big(t,I_v^*(t)\big)\right|<\mathbb{N}_7,
\end{aligned}\tag{28}$$

$\exists\ \big(S_h,E_h,I_h,R_h,S_v,E_v,I_v\big)\in\mathcal{M}$ satisfying the fractal-fractional model (11) with

$$\begin{cases}
\big|S_h^*-S_h\big|\le\mathcal{Q}_{\mathbf{M}_1}\mathbb{N}_1, & \big|E_h^*-E_h\big|\le\mathcal{Q}_{\mathbf{M}_2}\mathbb{N}_2,\\
\big|I_h^*-I_h\big|\le\mathcal{Q}_{\mathbf{M}_3}\mathbb{N}_3, & \big|R_h^*-R_h\big|\le\mathcal{Q}_{\mathbf{M}_4}\mathbb{N}_4,\\
\big|S_v^*-S_v\big|\le\mathcal{Q}\mathbf{M}_5\mathbb{N}_5, & \big|E_v^*-E_v\big|\le\mathcal{Q}\mathbf{M}_6\mathbb{N}_6,\\
\big|I_v^*-I_v\big|\le\mathcal{Q}\mathbf{M}_7\mathbb{N}_7.
\end{cases}$$

Remark 6.2. $\big(S_h^*,E_h^*,I_h^*,R_h^*,S_v^*,E_v^*,I_h^*\big)\in\mathcal{M}$ is termed as a solution for (28) iff $\exists\,\mathcal{G}_1^*,\dots\mathcal{G}_7^*\in\mathcal{C}([0,\tau],\mathbb{R})$ (based on $S_h^*,E_h^*,I_h^*,R_h^*,S_v^*,E_v^*,I_h^*$, respectively) so that $\forall\,t\in\mathcal{J}$,

(i) $|\mathcal{G}_j^*(t)|<\mathbb{N}_j$,

(ii) We have

$$\begin{cases}
{}^{\mathbf{FFML}}\mathcal{D}_{0,t}^{(\mu_*,\nu_*)}S_h^*(t)=\mathbf{M}_1\big(t,S_h^*(t)\big)+\mathcal{G}_1^*(t),\\
{}^{\mathbf{FFML}}\mathcal{D}_{0,t}^{(\mu_*,\nu_*)}E_h^*(t)=\mathbf{M}_2\big(t,E_h^*(t)\big)+\mathcal{G}_2^*(t),\\
{}^{\mathbf{FFML}}\mathcal{D}_{0,t}^{(\mu_*,\nu_*)}I_h^*(t)=\mathbf{M}_3\big(t,I_h^*(t)\big)+\mathcal{G}_3^*(t),\\
{}^{\mathbf{FFML}}\mathcal{D}_{0,t}^{(\mu_*,\nu_*)}R_h^*(t)=\mathbf{M}_4\big(t,R_h^*(t)\big)+\mathcal{G}_4^*(t),\\
{}^{\mathbf{FFML}}\mathcal{D}_{0,t}^{(\mu_*,\nu_*)}S_v^*(t)=\mathbf{M}_5\big(t,S_v^*(t)\big)+\mathcal{G}_5^*(t),\\
{}^{\mathbf{FFML}}\mathcal{D}_{0,t}^{(\mu_*,\nu_*)}E_v^*(t)=\mathbf{M}_6\big(t,E_v^*(t)\big)+\mathcal{G}_6^*(t),\\
{}^{\mathbf{FFML}}\mathcal{D}_{0,t}^{(\mu_*,\nu_*)}I_v^*(t)=\mathbf{M}_7\big(t,I_v^*(t)\big)+\mathcal{G}_7^*(t).
\end{cases}$$

Lemma 6.3. *For each $\mathbb{N}_1,\dots,\mathbb{N}_7>0$, suppose that $\big(S_h^*,E_h^*,I_h^*,R_h^*,S_v^*,E_v^*,I_h^*\big)\in\mathcal{M}$ is considered as a solution of (28). Then the functions $S_h^*,E_h^*,I_h^*,R_h^*,S_v^*,E_v^*,I_h^*\in\mathbb{W}$ satisfies the inequalities*

$$\begin{aligned}
&\Big|S_h^*(t)-\Big(S_{h0}+\frac{(1-\mu_*)\nu_*t^{\nu_*-1}}{\mathbf{G}(\mu_*)}\mathbf{M}_1(t,S_h^*(t))\\
&\quad+\frac{\mu_*\nu_*}{\Gamma(\mu_*)\mathbf{G}(\mu_*)}\int_0^t\mathfrak{s}^{\nu_*-1}(t-\mathfrak{s})^{\mu_*-1}\mathbf{M}_1(\mathfrak{s},S_h^*(\mathfrak{s}))\,\mathrm{d}\mathfrak{s}\Big)\Big|\\
&\quad\le\Big[\frac{(1-\mu_*)\nu_*\tau^{\nu_*-1}}{\mathbf{G}(\mu_*)}+\frac{\mu_*\nu_*\Gamma(\nu_*)\tau^{\mu_*+\nu_*-1}}{\Gamma(\mu_*+\nu_*)\mathbf{G}(\mu_*)}\Big]\mathbb{N}_1,
\end{aligned}\tag{29}$$

$$\begin{aligned}
&\Big|E_h^*(t)-\Big(E_{v0}+\frac{(1-\mu_*)\nu_*t^{\nu_*-1}}{\mathbf{G}(\mu_*)}\mathbf{M}_2(t,E_v^*(t))\\
&\quad+\frac{\mu_*\nu_*}{\Gamma(\mu_*)\mathbf{G}(\mu_*)}\int_0^t\mathfrak{s}^{\nu_*-1}(t-\mathfrak{s})^{\mu_*-1}\mathbf{M}_2(\mathfrak{s},E_v^*(\mathfrak{s}))\,\mathrm{d}\mathfrak{s}\Big)\Big|\\
&\quad\le\Big[\frac{(1-\mu_*)\nu_*\tau^{\nu_*-1}}{\mathbf{G}(\mu_*)}+\frac{\mu_*\nu_*\Gamma(\nu_*)\tau^{\mu_*+\nu_*-1}}{\Gamma(\mu_*+\nu_*)\mathbf{G}(\mu_*)}\Big]\mathbb{N}_2,
\end{aligned}\tag{30}$$

$$\begin{aligned}
&\Big|I_h^*(t)-\Big(I_{h0}+\frac{(1-\mu_*)\nu_*t^{\nu_*-1}}{\mathbf{G}(\mu_*)}\mathbf{M}_3(t,I_h^*(t))\\
&\quad+\frac{\mu_*\nu_*}{\Gamma(\mu_*)\mathbf{G}(\mu_*)}\int_0^t\mathfrak{s}^{\nu_*-1}(t-\mathfrak{s})^{\mu_*-1}\mathbf{M}_3(\mathfrak{s},I_h^*(\mathfrak{s}))\,\mathrm{d}\mathfrak{s}\Big)\Big|\\
&\quad\le\Big[\frac{(1-\mu_*)\nu_*\tau^{\nu_*-1}}{\mathbf{G}(\mu_*)}+\frac{\mu_*\nu_*\Gamma(\nu_*)\tau^{\mu_*+\nu_*-1}}{\Gamma(\mu_*+\nu_*)\mathbf{G}(\mu_*)}\Big]\mathbb{N}_3,
\end{aligned}\tag{31}$$

$$\left|R_h^*(t)-\left(R_{h0}+\frac{(1-\mu_*)\nu_* t^{\nu_*-1}}{\mathbf{G}(\mu_*)}\mathbf{M}_4(t,R_h^*(t))\right.\right.$$
$$\left.\left.+\frac{\mu_*\nu_*}{\Gamma(\mu_*)\mathbf{G}(\mu_*)}\int_0^t \mathfrak{s}^{\nu_*-1}(t-\mathfrak{s})^{\mu_*-1}\mathbf{M}_4(\mathfrak{s},R_h^*(\mathfrak{s}))\,\mathrm{d}\mathfrak{s}\right)\right|$$
$$\le\left[\frac{(1-\mu_*)\nu_*\tau^{\nu_*-1}}{\mathbf{G}(\mu_*)}+\frac{\mu_*\nu_*\Gamma(\nu_*)\tau^{\mu_*+\nu_*-1}}{\Gamma(\mu_*+\nu_*)\mathbf{G}(\mu_*)}\right]\mathbb{N}_4, \tag{32}$$

$$\left|S_v^*(t)-\left(S_{v0}+\frac{(1-\mu_*)\nu_* t^{\nu_*-1}}{\mathbf{G}(\mu_*)}\mathbf{M}_5(t,S_v^*(t))\right.\right.$$
$$\left.\left.+\frac{\mu_*\nu_*}{\Gamma(\mu_*)\mathbf{G}(\mu_*)}\int_0^t \mathfrak{s}^{\nu_*-1}(t-\mathfrak{s})^{\mu_*-1}\mathbf{M}_5(\mathfrak{s},R^*(\mathfrak{s}))\,\mathrm{d}\mathfrak{s}\right)\right|$$
$$\le\left[\frac{(1-\mu_*)\nu_*\tau^{\nu_*-1}}{\mathbf{G}(\mu_*)}+\frac{\mu_*\nu_*\Gamma(\nu_*)\tau^{\mu_*+\nu_*-1}}{\Gamma(\mu_*+\nu_*)\mathbf{G}(\mu_*)}\right]\mathbb{N}_5, \tag{33}$$

$$\left|E_v^*(t)-\left(E_{v0}+\frac{(1-\mu_*)\nu_* t^{\nu_*-1}}{\mathbf{G}(\mu_*)}\mathbf{M}_6(t,E_v^*(t))\right.\right.$$
$$\left.\left.+\frac{\mu_*\nu_*}{\Gamma(\mu_*)\mathbf{G}(\mu_*)}\int_0^t \mathfrak{s}^{\nu_*-1}(t-\mathfrak{s})^{\mu_*-1}\mathbf{M}_6(\mathfrak{s},E_v^*(\mathfrak{s}))\,\mathrm{d}\mathfrak{s}\right)\right|$$
$$\le\left[\frac{(1-\mu_*)\nu_*\tau^{\nu_*-1}}{\mathbf{G}(\mu_*)}+\frac{\mu_*\nu_*\Gamma(\nu_*)\tau^{\mu_*+\nu_*-1}}{\Gamma(\mu_*+\nu_*)\mathbf{G}(\mu_*)}\right]\mathbb{N}_6, \tag{34}$$

$$\left|I_v^*(t)-\left(I_{v0}+\frac{(1-\mu_*)\nu_* t^{\nu_*-1}}{\mathbf{G}(\mu_*)}\mathbf{M}_7(t,I_v^*(t))\right.\right.$$
$$\left.\left.+\frac{\mu_*\nu_*}{\Gamma(\mu_*)\mathbf{G}(\mu_*)}\int_0^t \mathfrak{s}^{\nu_*-1}(t-\mathfrak{s})^{\mu_*-1}\mathbf{M}_7(\mathfrak{s},I_v^*(\mathfrak{s}))\,\mathrm{d}\mathfrak{s}\right)\right|$$
$$\le\left[\frac{(1-\mu_*)\nu_*\tau^{\nu_*-1}}{\mathbf{G}(\mu_*)}+\frac{\mu_*\nu_*\Gamma(\nu_*)\tau^{\mu_*+\nu_*-1}}{\Gamma(\mu_*+\nu_*)\mathbf{G}(\mu_*)}\right]\mathbb{N}_7. \tag{35}$$

Proof. Let $\mathbb{N}_1>0$ be arbitrary. Since $S_h^*\in\mathbb{W}$ satisfies

$$\left|{}^{\mathbf{FFML}}\mathcal{D}_{0,t}^{(\mu_*,\nu_*)}S_h^*(t)-\mathbf{M}_1\big(t,S_h^*(t)\big)\right|<\mathbb{N}_1,$$

so, by Remark 6.2, we are free to choose a function $\mathcal{G}_1^*(t)$ so that

$${}^{\mathbf{FFML}}\mathcal{D}_{0,t}^{(\mu_*,\nu_*)}S_h^*(t)=\mathbf{M}_1\big(t,S_h^*(t)\big)+\mathcal{G}_1^*(t),$$

and $|\mathcal{G}_1^*(t)|\le\mathbb{N}_1$. It follows that

$$S_h^*(t)=S_{h0}+\frac{(1-\mu_*)\nu_* t^{\nu_*-1}}{\mathbf{G}(\mu_*)}\Big[\mathbf{M}_1(t,S_h^*(t))+\mathcal{G}_1^*(t)\Big]$$
$$+\frac{\mu_*\nu_*}{\Gamma(\mu_*)\mathbf{G}(\mu_*)}\int_0^t \mathfrak{s}^{\nu_*-1}(t-\mathfrak{s})^{\mu_*-1}\Big[\mathbf{M}_1(\mathfrak{s},S_h^*(\mathfrak{s}))+\mathcal{G}_1^*(\mathfrak{s})\Big]\,\mathrm{d}\mathfrak{s}.$$

Then, we estimate

$$\left|S_h^*(t)-\left(S_{h0}+\frac{(1-\mu_*)\nu_* t^{\nu_*-1}}{\mathbf{G}(\mu_*)}\mathbf{M}_1(t,S_h^*(t))\right.\right.$$
$$\left.\left.+\frac{\mu_*\nu_*}{\Gamma(\mu_*)\mathbf{G}(\mu_*)}\int_0^t \mathfrak{s}^{\nu_*-1}(t-\mathfrak{s})^{\mu_*-1}\mathbf{M}_1(\mathfrak{s},S_h^*(\mathfrak{s}))\,\mathrm{d}\mathfrak{s}\right)\right|$$
$$\le\frac{(1-\mu_*)\nu_* t^{\nu_*-1}}{\mathbf{G}(\mu_*)}|\mathcal{G}_1^*(t)|+\frac{\mu_*\nu_*}{\Gamma(\mu_*)\mathbf{G}(\mu_*)}\int_0^t \mathfrak{s}^{\nu_*-1}(t-\mathfrak{s})^{\mu_*-1}|\mathcal{G}_1^*(\mathfrak{s})|\,\mathrm{d}\mathfrak{s}$$
$$\le\frac{(1-\mu_*)\nu_*\tau^{\nu_*-1}}{\mathbf{G}(\mu_*)}\mathbb{N}_1+\frac{\mu_*\nu_*\tau^{\mu_*+\nu_*-1}\Gamma(\nu_*)}{\Gamma(\mu_*+\nu_*)\mathbf{G}(\mu_*)}\mathbb{N}_1$$
$$=\left[\frac{(1-\mu_*)\nu_*\tau^{\nu_*-1}}{\mathbf{G}(\mu_*)}+\frac{\mu_*\nu_*\Gamma(\nu_*)\tau^{\mu_*+\nu_*-1}}{\Gamma(\mu_*+\nu_*)\mathbf{G}(\mu_*)}\right]\mathbb{N}_1.$$

This means that the inequality (29) is achieved. Similarly, we can obtain the inequalities (30)–(35). □

Here, we check the UH-stability of the fractal-fractional model (11) .

Theorem 6.4. *Let* (**V**3) *be satisfied. Then the fractal-fractional model* (11) *is UH-stable on* $\mathcal{J} := [0, \tau]$ *such that*

$$\Big[\frac{(1-\mu_*)\nu_*\tau^{\nu_*-1}}{\mathbf{G}(\mu_*)} + \frac{\mu_*\nu_*\Gamma(\nu_*)\tau^{\mu_*+\nu_*-1}}{\Gamma(\mu_*+\nu_*)\mathbf{G}(\mu_*)}\Big]\mathbf{L}_J^* < 1, \quad J \in \{1, \dots, 7\},$$

in which $\mathbf{L}_j^*$*'s are introduced by* (26).

Proof. Let $\mathbb{N}_1 > 0$ and $S_h^* \in \mathbb{W}$ be an arbitrary solution of (28). Also, from Theorem 5.4, we assume $S_h \in \mathbb{W}$ as a unique solution of the fractal-fractional model (11). Therefore $S_h(t)$ is defined as

$$\begin{aligned} S_h(t) = S_h(0) &+ \frac{(1-\mu_*)\nu_* t^{\nu_*-1}}{\mathbf{G}(\mu_*)}\mathbf{M}_1(t, S_h(t)) \\ &+ \frac{\mu_*\nu_*}{\Gamma(\mu_*)\mathbf{G}(\mu_*)}\int_0^t \mathfrak{s}^{\nu_*-1}(t-\mathfrak{s})^{\mu_*-1}\mathbf{M}_1(\mathfrak{s}, S_h(\mathfrak{s}))\,\mathrm{d}\mathfrak{s}. \end{aligned}$$

Therefore, by Lemma 6.3 and with the help of the triangle inequality, we estimate

$$\begin{aligned} \big|S_h^*(t) - S_h(t)\big| &\le \Big|S_h^*(t) - S_{h0} - \frac{(1-\mu_*)\nu_* t^{\nu_*-1}}{\mathbf{G}(\mu_*)}\mathbf{M}_1(t, S_h(t)) \\ &\quad - \frac{\mu_*\nu_*}{\Gamma(\mu_*)\mathbf{G}(\mu_*)}\int_0^t \mathfrak{s}^{\nu_*-1}(t-\mathfrak{s})^{\mu_*-1}\mathbf{M}_1(\mathfrak{s}, S_h(\mathfrak{s}))\,\mathrm{d}\mathfrak{s}\Big| \\ &\le \Big|S_h^*(t) - \Big(S_{h0} + \frac{(1-\mu_*)\nu_* t^{\nu_*-1}}{\mathbf{G}(\mu_*)}\mathbf{M}_1(t, S_h^*(t)) \\ &\quad + \frac{\mu_*\nu_*}{\Gamma(\mu_*)\mathbf{G}(\mu_*)}\int_0^t \mathfrak{s}^{\nu_*-1}(t-\mathfrak{s})^{\mu_*-1}\mathbf{M}_1(\mathfrak{s}, S_h^*(\mathfrak{s}))\,\mathrm{d}\mathfrak{s}\Big)\Big| \\ &\quad + \frac{(1-\mu_*)\nu_* t^{\nu_*-1}}{\mathbf{G}(\mu_*)}\big|\mathbf{M}_1(t, S_h^*(t)) - \mathbf{M}_1(t, S_h(t))\big| \\ &\quad + \frac{\mu_*\nu_*}{\Gamma(\mu_*)\mathbf{G}(\mu_*)}\int_0^t \mathfrak{s}^{\nu_*-1}(t-\mathfrak{s})^{\mu_*-1}\big|\mathbf{M}_1(\mathfrak{s}, S_h^*(\mathfrak{s})) - \mathbf{M}_1(\mathfrak{s}, S_h(\mathfrak{s}))\big|\,\mathrm{d}\mathfrak{w} \\ &\le \Big[\frac{(1-\mu_*)\nu_*\tau^{\nu_*-1}}{\mathbf{G}(\mu_*)} + \frac{\mu_*\nu_*\Gamma(\nu_*)\tau^{\mu_*+\nu_*-1}}{\Gamma(\mu_*+\nu_*)\mathbf{G}(\mu_*)}\Big]\mathbb{N}_1 + \frac{(1-\mu_*)\nu_*\tau^{\nu_*-1}}{\mathbf{G}(\mu_*)}\mathbf{L}_1^*\|S_h^* - S_h\| \\ &\quad + \frac{\mu_*\nu_*\tau^{\mu_*+\nu_*-1}\Gamma(\nu_*)}{\Gamma(\mu_*+\nu_*)\mathbf{G}(\mu_*)}\mathbf{L}_1^*\|S_h^* - S_h\| \\ &\le \Big[\frac{(1-\mu_*)\nu_*\tau^{\nu_*-1}}{\mathbf{G}(\mu_*)} + \frac{\mu_*\nu_*\Gamma(\nu_*)\tau^{\mu_*+\nu_*-1}}{\Gamma(\mu_*+\nu_*)\mathbf{G}(\mu_*)}\Big]\mathbb{N}_1 \\ &\quad + \Big[\frac{(1-\mu_*)\nu_*\tau^{\nu_*-1}}{\mathbf{G}(\mu_*)} + \frac{\mu_*\nu_*\Gamma(\nu_*)\tau^{\mu_*+\nu_*-1}}{\Gamma(\mu_*+\nu_*)\mathbf{G}(\mu_*)}\Big]\mathbf{L}_1^*\|S_h^* - S_h\|. \end{aligned}$$

Hence, we get

$$\|S_h^* - S_h\| \le \frac{\Big[\frac{(1-\mu_*)\nu_*\tau^{\nu_*-1}}{\mathbf{G}(\mu_*)} + \frac{\mu_*\nu_*\Gamma(\nu_*)\tau^{\mu_*+\nu_*-1}}{\Gamma(\mu_*+\nu_*)\mathbf{G}(\mu_*)}\Big]\mathbb{N}_1}{1 - \Big[\frac{(1-\mu_*)\nu_*\tau^{\nu_*-1}}{\mathbf{G}(\mu_*)} + \frac{\mu_*\nu_*\Gamma(\nu_*)\tau^{\mu_*+\nu_*-1}}{\Gamma(\mu_*+\nu_*)\mathbf{G}(\mu_*)}\Big]\mathbf{L}_1^*}.$$

If we let $\mathcal{Q}_{\mathbf{M}_1} = \dfrac{\Big[\frac{(1-\mu_*)\nu_*\tau^{\nu_*-1}}{\mathbf{G}(\mu_*)} + \frac{\mu_*\nu_*\Gamma(\nu_*)\tau^{\mu_*+\nu_*-1}}{\Gamma(\mu_*+\nu_*)\mathbf{G}(\mu_*)}\Big]}{1 - \Big[\frac{(1-\mu_*)\nu_*\tau^{\nu_*-1}}{\mathbf{G}(\mu_*)} + \frac{\mu_*\nu_*\Gamma(\nu_*)\tau^{\mu_*+\nu_*-1}}{\Gamma(\mu_*+\nu_*)\mathbf{G}(\mu_*)}\Big]\mathbf{L}_1^*}$, then $\|S_h^* - S_h\| \le \mathcal{Q}\mathbf{M}_1\mathbb{N}_1$. In the same step, we have

$$\|E_h^* - E_h\| \le \mathcal{Q}\mathbf{M}_2\mathbb{N}_2,$$

$$\|I_h^* - I_h\| \le \mathcal{Q}\mathbf{M}_3\mathbb{N}_3,$$

$$\|R_h^* - R_h\| \le \mathcal{Q}\mathbf{M}_4\mathbb{N}_4,$$

$$\|S_v^* - S_v\| \le \mathcal{Q}\mathbf{M}_5\mathbb{N}_5,$$

$$\|E_v^* - E_v\| \leq \mathcal{Q}\mathbf{M}_6\mathbb{N}_6,$$

$$\|I_v^* - I_v\| \leq \mathcal{Q}\mathbf{M}_7\mathbb{N}_7,$$

where

$$\mathcal{Q}\mathbf{M}_j = \frac{\left[\frac{(1-\mu_*)\nu_*\tau^{\nu_*-1}}{\mathbf{G}(\mu_*)} + \frac{\mu_*\nu_*\Gamma(\nu_*)\tau^{\mu_*+\nu_*-1}}{\Gamma(\mu_*+\nu_*)\mathbf{G}(\mu_*)}\right]}{1-\left[\frac{(1-\mu_*)\nu_*\tau^{\nu_*-1}}{\mathbf{G}(\mu_*)} + \frac{\mu_*\nu_*\Gamma(\nu_*)\tau^{\mu_*+\nu_*-1}}{\Gamma(\mu_*+\nu_*)\mathbf{G}(\mu_*)}\right]\mathbf{L}_j^*}, \quad (j \in \{2,\ldots,7\}).$$

Hence, the UH-stability of the fractal-fractional model (11) is fulfilled. □

7. Numerical scheme

In this section, we provide the numerical schemes for our considered fractal-fractional Zika virus transmission model base on the Newton polynomial approximation with reference to [84]. We consider the Cauchy problem of the ABC derivative as follows;

$$\begin{cases} {}^{ABC}D_t^{\mu_*\nu_*}\Upsilon(t) = \Psi(t,\Upsilon(t)), \\ \Upsilon(0) = \Upsilon_0. \end{cases} \tag{36}$$

By employing the initial condition together with the operator ${}^{ABC}I_0^{\mu_*\nu_*}$, we convert the Cauchy problem (36) to fractal-fractional ABC integral equations as

$$\Upsilon(t) = \Upsilon(0) + \frac{\nu_*(1-\mu_*)t^{\nu_*-1}}{\mathbf{G}(\mu_*)}\Psi(t,\Upsilon(t)) + \frac{\mu_*\nu_*}{\mathbf{G}(\mu_*)\Gamma(\mu_*)}\int_0^t s^{\nu_*-1}(t-s)^{\mu_*-1}\Psi(s,\Upsilon(s))ds. \tag{37}$$

Taking the point $t_{(z^*+1)} = (z^*+1)h$ and $t_{z^*} = z^*h$, $z^* = 0,1,2,\ldots$, with h being the time step, and also letting $\aleph(t,\Upsilon(t)) = \nu_* t^{\nu_*-1}\Psi(t,\Upsilon(t))$, then, we can simple get

$$\Upsilon(t_{(z^*+1)}) = \Upsilon(0) + \frac{(1-\mu_*)}{\mathbf{G}(\mu_*)}\aleph(t,\Upsilon(t)) + \frac{\mu_*}{\mathbf{G}(\mu_*)\Gamma(\mu_*)}\int_0^{t_{z^*+1}}(t_{(z^*+1)}-s)^{\mu_*-1}\aleph(s,\Upsilon(s))ds. \tag{38}$$

For simplicity, we can rewrite as

$$\begin{aligned}\Upsilon(t_{(z^*+1)}) = \Upsilon(0) &+ \frac{(1-\mu_*)}{\mathbf{G}(\mu_*)}\aleph(t_{z^*},\Upsilon^{t_{z^*}}) + \frac{\mu_*}{\mathbf{G}(\mu_*)\Gamma(\mu_*)} \\ &\times \sum_{r^*=2}^{z^*}\int_{t_{r^*}}^{t_{r^*+1}}(t_{(z^*+1)}-s)^{\mu_*-1}\aleph(s,\Upsilon(s))ds.\end{aligned} \tag{39}$$

Now, using the Newton polynomial, (39) can be written as

$$\begin{aligned}\Upsilon^{z^*+1} = \Upsilon(0) &+ \frac{(1-\mu_*)}{\mathbf{G}(\mu_*)}\aleph(t_{z^*},\Upsilon^{t_{z^*}}) + \frac{\mu_*}{\mathbf{G}(\mu_*)\Gamma(\mu_*)} \\ &\times \sum_{r^*=2}^{z^*}\Bigg[\int_{t_{r^*}}^{t_{r^*+1}}(t_{z^*+1}-s)^{\mu_*-1}\aleph(t_{z^*-2},\Upsilon^{z^*-2})ds \\ &+ \int_{t_{r^*}}^{t_{r^*+1}}\frac{\aleph(t_{r^*-1},\Upsilon^{r^*-1}) - \aleph(t_{r^*-2},\Upsilon^{r^*-2})}{h} \\ &\times (s-t_{r^*-2})(t_{z^*+1}-s)^{\mu_*-1} \\ &+ \int_{t_{r^*}}^{t_{r^*+1}}\frac{\aleph(t_{r^*},\Upsilon^{r^*}) - 2\aleph(t_{r^*-1},\Upsilon^{r^*-1}) + \aleph(t_{r^*-2},\Upsilon^{r^*-2})}{2h^2} \\ &\times (s-t_{r^*-1})(s-t_{r^*-2})(t_{(z^*+1)}-s)^{\mu_*-1}ds\Bigg].\end{aligned} \tag{40}$$

For simplicity (40)is written as

$$\begin{aligned}\Upsilon^{z^*+1} = \Upsilon(0) &+ \frac{(1-\mu_*)}{\mathbf{G}(\mu_*)}\aleph(t_{z^*},\Upsilon^{z^*}) + \frac{\mu_*}{\mathbf{G}(\mu_*)\Gamma(\mu_*)}\sum_{r^*=2}^{z^*}\aleph(t_{r^*+2},\Upsilon^{r^*-2}) \\ &\times \sum_{r^*=2}^{z^*}\int_{t_{r^*}}^{t_{r^*+1}}(t_{(z^*+1)}-s)^{\mu_*-1}ds\end{aligned}$$

$$
\begin{aligned}
&+\frac{\mu_*}{\mathbf{G}(\mu_*)\Gamma(\mu_*)}\sum_{r^*=2}^{z^*}\frac{\aleph(t_{r^*-1},\Upsilon^{r^*-1})-\aleph(t_{r^*-2},\Upsilon^{r^*-2})}{h}\\
&\times\int_{t_{r^*}}^{t_{r^*+1}}(s-t_{r^*-2})(t_{(z^*+1)}-s)^{\mu_*-1}\\
&+\frac{\mu_*}{\mathbf{G}(\mu_*)\Gamma(\mu_*)}\sum_{r^*=2}^{z^*}\frac{\aleph(t_{r^*},\Upsilon^{r^*})-2\aleph(t_{r^*-1},\Upsilon^{r^*-1})+\aleph(t_{r^*-2},\Upsilon^{r^*-2})}{2h^2}\\
&\times\int_{t_{r^*}}^{t_{r^*+1}}(s-t_{r^*-1})(s-t_{r^*-2})(t_{(z^*+1)}-s)^{\mu_*-1}ds.
\end{aligned}
\tag{41}
$$

For further breakdown of (41), we get the following approximation

$$
\begin{aligned}
\Upsilon^{z^*+1}&=\Upsilon(0)+\frac{(1-\mu_*)}{\mathbf{G}(\mu_*)}\aleph(t_{z^*},\Upsilon^{z^*})+\frac{\mu_*h_*^{\mu}}{\mathbf{G}(\mu_*)\Gamma(\mu_*+1)}\sum_{r^*=2}^{z^*}\aleph(t_{r^*+2},\Upsilon^{r^*-2})\\
&\times\left[(z^*-m^*+1)^{\mu_*}-(z^*-m^*)^{\mu_*}\right]\\
&+\frac{\mu_*h_*^{\mu}}{\mathbf{G}(\mu_*)\Gamma(\mu_*+2)}\sum_{r^*=2}^{z^*}\left[\aleph(t_{r^*-1},\Upsilon^{r^*-1})-\aleph(t_{r^*-2},\Upsilon^{r^*-2})\right]\\
&\times\left[(z^*-m^*+1)^{\mu_*}(z^*-m^*+3+2\mu_*)-(z^*-m^*)^{\mu_*}(z^*-m^*+3+3\mu_*)\right]\\
&+\frac{\mu_*h_*^{\mu}}{2\mathbf{G}(\mu_*)\Gamma(\mu_*+3)}\sum_{r^*=2}^{z^*}\left[\aleph(t_{r^*},\Upsilon^{r^*})-2\aleph(t_{r^*-1},\Upsilon^{r^*-1})+\aleph(t_{r^*-2},\Upsilon^{r^*-2})\right]\\
&\times\Big[(z^*-m^*+1)^{\mu_*}[2(z^*-m^*)^2+(3\mu_*-10)(z^*-m^*)+2\mu_*^2+9\mu_*+12]\\
&-(z^*-m^*)^{\mu_*}[2(z^*-m^*)^2+(5\mu_*-10)(z^*-m^*)+6\mu_*^2+18\mu_*+12]\Big].
\end{aligned}
\tag{42}
$$

We now substitute back $\aleph(t,\Upsilon(t))=\nu_*t^{\nu_*-1}\Psi(t,\Upsilon(t))$ into (42), then, we simply get general Newton numerical scheme for our propose model (11)

$$
\begin{aligned}
\Upsilon^{z^*+1}&=\Upsilon(0)+\frac{(1-\mu_*)}{\mathbf{G}(\mu_*)}\nu_*t_{z^*}^{\nu_*-1}\Psi(t_{z^*},\Upsilon(t))+\frac{\mu_*h_*^{\mu}}{\mathbf{G}(\mu_*)\Gamma(\mu_*+1)}\sum_{r^*=2}^{z^*}\nu_*t_{r^*-2}^{\nu_*-1}\Psi(t_{r^*-2},\Upsilon^{r^*-2})\\
&\times\left[(z^*-m^*+1)^{\mu_*}-(z^*-m^*)^{\mu_*}\right]\\
&+\frac{\mu_*h_*^{\mu}}{\mathbf{G}(\mu_*)\Gamma(\mu_*+2)}\sum_{r^*=2}^{z^*}\left[\nu_*t_{r^*-1}^{\nu_*-1}\Psi(t_{r^*-1},\Upsilon^{r^*-1})-\nu_*t_{r^*-2}^{\nu_*-1}\Psi(t_{r^*-2},\Upsilon^{r^*-2})\right]\\
&\times\left[(z^*-m^*+1)^{\mu_*}(z^*-m^*+3+2\mu_*)-(z^*-m^*)^{\mu_*}(z^*-m^*+3+3\mu_*)\right]\\
&+\frac{\mu_*h_*^{\mu}}{2\mathbf{G}(\mu_*)\Gamma(\mu_*+3)}\sum_{r^*=2}^{z^*}\left[\nu_*t_{r^*}^{\nu_*-1}\Psi(t_{r^*},\Upsilon^{r^*})-2\nu_*t_{r^*-1}^{\nu_*-1}\Psi(t_{r^*-1},\Upsilon^{r^*-1})+\nu_*t_{r^*-2}^{\nu_*-1}\Psi(t_{r^*-2},\Upsilon^{r^*-2})\right]\\
&\times\Big[(z^*-m^*+1)^{\mu_*}[2(z^*-m^*)^2+(3\mu_*-10)(z^*-m^*)+2\mu_*^2+9\mu_*+12]\\
&-(z^*-m^*)^{\mu_*}[2(z^*-m^*)^2+(5\mu_*-10)(z^*-m^*)+6\mu_*^2+18\mu_*+12]\Big].
\end{aligned}
\tag{43}
$$

Now for simplicity we rewrite fractal-fractional Zika virus model (11) as

$$
\begin{cases}
{}^{FABC}D_t^{\mu_*,\nu_*}S_h(t)=M_1(t,S_h,E_h,I_h,R_h,S_v,E_v,I_v),\\
{}^{FABC}D_t^{\mu_*,\nu_*}E_h(t)=M_2(t,S_h,E_h,I_h,R_h,S_v,E_v,I_v),\\
{}^{FABC}D_t^{\mu_*,\nu_*}I_h(t)=M_3(t,S_h,E_h,I_h,R_h,S_v,E_v,I_v),\\
{}^{FABC}D_t^{\mu_*,\nu_*}R_h(t)=M_4(t,S_h,E_h,I_h,R_h,S_v,E_v,I_v),\\
{}^{FABC}D_t^{\mu_*,\nu_*}S_v(t)=M_5(t,S_h,E_h,I_h,R_h,S_v,E_v,I_v),\\
{}^{FABC}D_t^{\mu_*,\nu_*}E_v(t)=M_6(t,S_h,E_h,I_h,R_h,S_v,E_v,I_v),\\
{}^{FABC}D_t^{\mu_*,\nu_*}I_v(t)=M_7(t,S_h,E_h,I_h,R_h,S_v,E_v,I_v),
\end{cases}
\tag{44}
$$

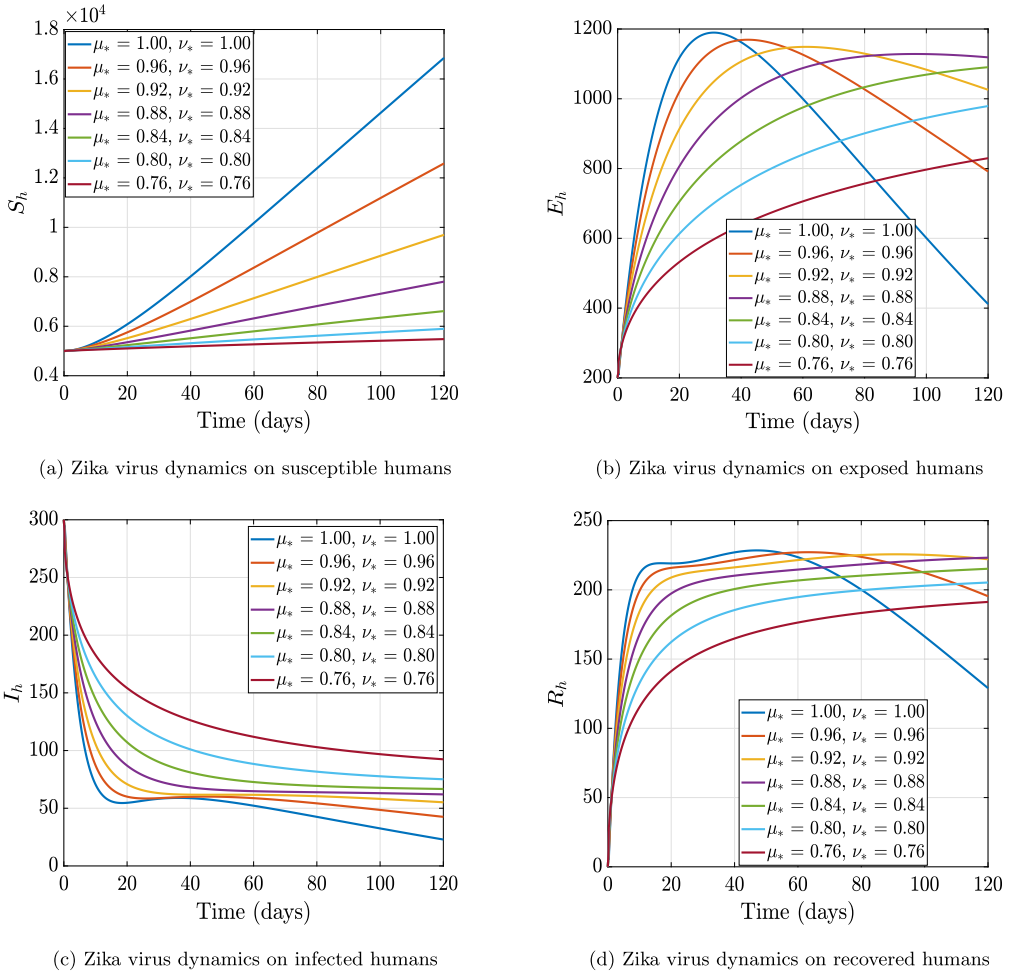

(a) Zika virus dynamics on susceptible humans

(b) Zika virus dynamics on exposed humans

(c) Zika virus dynamics on infected humans

(d) Zika virus dynamics on recovered humans

Fig. 1. Numerical dynamics of Zika transmission under the ABC fractal-fractional operator for humans.

Therefore, the fractal-fractional Zika virus numerical scheme base on Newton polynomial is as follows

$$
\begin{aligned}
S_h^{z^*+1} &= S_h(0) + \frac{(1-\mu_*)}{\mathbf{G}(\mu_*)}\nu_* t_{z^*}^{\nu_*-1} M_1(t_n, S_h^n, E_h^n, I_h^n, R_h^n, S_v^n, E_v^n, I_v^n) + \frac{\mu_* h_*^{\mu}}{\mathbf{G}(\mu_*)\Gamma(\mu_*+1)} \\
&\sum_{r^*=2}^{z^*} \nu_* t_{r^*-2}^{\nu_*-1} M_1(t_{r^*-2}, S_h^{r^*-2}, E_h^{r^*-2}, I_h^{r^*-2}, R_h^{r^*-2}, S_v^{r^*-2}, E_v^{r^*-2}, I_v^{r^*-2}) \\
&\times \left[(z^*-m^*+1)^{\mu_*} - (z^*-m^*)^{\mu_*}\right] \\
&+ \frac{\mu_* h_*^{\mu}}{\mathbf{G}(\mu_*)\Gamma(\mu_*+2)} \sum_{r^*=2}^{z^*} \Big[\nu_* t_{r^*-1}^{\nu_*-1} M_1(t_{r^*-1}, S_h^{r^*-1}, E_h^{r^*-1}, I_h^{r^*-1}, R_h^{r^*-1}, S_v^{r^*-1}, E_v^{r^*-1}, I_v^{r^*-1}) \\
&- \nu_* t_{r^*-2}^{\nu_*-1} M_1(t_{r^*-2}, S_h^{r^*-2}, E_h^{r^*-2}, I_h^{r^*-2}, R_h^{r^*-2}, S_v^{r^*-2}, E_v^{r^*-2}, I_v^{r^*-2}) \Big] \\
&\times \left[(z^*-m^*+1)^{\mu_*}(z^*-m^*+3+2\mu_*) - (z^*-m^*)^{\mu_*}(z^*-m^*+3+3\mu_*)\right] \\
&+ \frac{\mu_* h_*^{\mu}}{2\mathbf{G}(\mu_*)\Gamma(\mu_*+3)} \sum_{r^*=2}^{z^*} \Big[\nu_* t_{r^*}^{\nu_*-1} M_1(t_{r^*}, S_h^{r^*}, E_h^{r^*}, I_h^{r^*}, R_h^{r^*}, S_v^{r^*}, E_v^{r^*}, I_v^{r^*}, T_m^{r^*}) \\
&- 2\nu_* t_{r^*-1}^{\nu_*-1} M_1(t_{r^*-1}, S_h^{r^*-1}, E_h^{r^*-1}, I_h^{r^*-1}, R_h^{r^*-1}, S_v^{r^*-1}, E_v^{r^*-1}, I_v^{r^*-1}) \\
&+ \nu_* t_{r^*-2}^{\nu_*-1} M_1(t_{r^*-2}, S_h^{r^*-2}, E_h^{r^*-2}, I_h^{r^*-2}, R_h^{r^*-2}, S_v^{r^*-2}, E_v^{r^*-2}, I_v^{r^*-2}) \Big] \\
&\times \Big[(z^*-m^*+1)^{\mu_*}[2(z^*-m^*)^2 + (3\mu_*-10)(z^*-m^*) + 2\mu_*^2 + 9\mu_* + 12] \\
&- (z^*-m^*)^{\mu_*}[2(z^*-m^*)^2 + (5\mu_*-10)(z^*-m^*) + 6\mu_*^2 + 18\mu_* + 12] \Big].
\end{aligned}
\tag{45}
$$

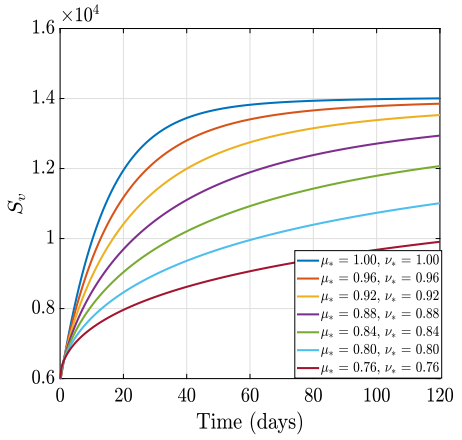

(a) Zika virus dynamics on susceptible mosquitoes

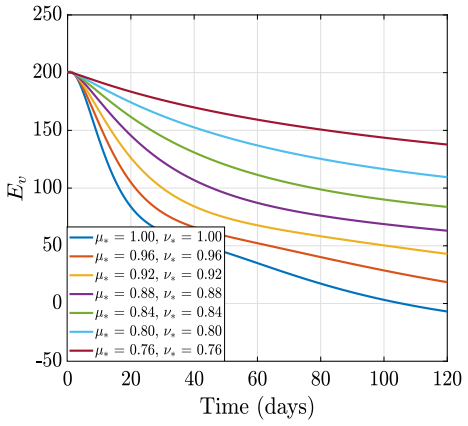

(b) Zika virus dynamics on exposed mosquitoes

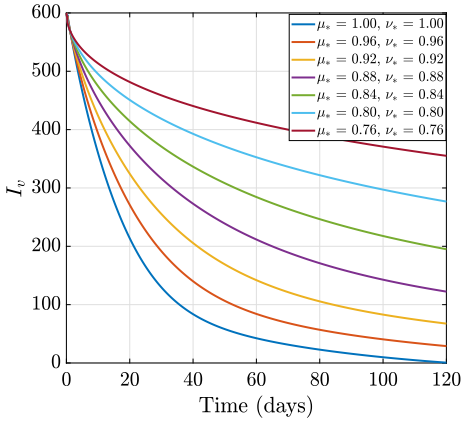

(c) Zika virus dynamics on infected mosquitoes

Fig. 2. Numerical dynamics of Zika transmission under the ABC fractal-fractional operator for the mosquito population.

$$
\begin{aligned}
E_h^{z^*+1} &= E_h(0) + \frac{(1-\mu_*)}{\mathbf{G}(\mu_*)} \nu_* t_{z^*}^{\nu_*-1} M_2(t_n, S_h^n, E_h^n, I_h^n, R_h^n, S_v^n, E_v^n, I_v^n) + \frac{\mu_* h_*^{\mu}}{\mathbf{G}(\mu_*)\Gamma(\mu_*+1)} \\
&\sum_{r^*=2}^{z^*} \nu_* t_{r^*-2}^{\nu_*-1} M_2(t_{r^*-2}, S_h^{r^*-2}, E_h^{r^*-2}, I_h^{r^*-2}, R_h^{r^*-2}, S_v^{r^*-2}, E_v^{r^*-2}, I_v^{r^*-2}) \\
&\times \left[(z^*-m^*+1)^{\mu_*} - (z^*-m^*)^{\mu_*}\right] \\
&+ \frac{\mu_* h_*^{\mu}}{\mathbf{G}(\mu_*)\Gamma(\mu_*+2)} \sum_{r^*=2}^{z^*} \Big[\nu_* t_{r^*-1}^{\nu_*-1} M_2(t_{r^*-1}, S_h^{r^*-1}, E_h^{r^*-1}, I_h^{r^*-1}, R_h^{r^*-1}, S_v^{r^*-1}, E_v^{r^*-1}, I_v^{r^*-1}) \\
&- \nu_* t_{r^*-2}^{\nu_*-1} M_2(t_{r^*-2}, S_h^{r^*-2}, E_h^{r^*-2}, I_h^{r^*-2}, R_h^{r^*-2}, S_v^{r^*-2}, E_v^{r^*-2}, I_v^{r^*-2}) \Big] \\
&\times \left[(z^*-m^*+1)^{\mu_*}(z^*-m^*+3+2\mu_*) - (z^*-m^*)^{\mu_*}(z^*-m^*+3+3\mu_*)\right] \\
&+ \frac{\mu_* h_*^{\mu}}{2\mathbf{G}(\mu_*)\Gamma(\mu_*+3)} \sum_{r^*=2}^{z^*} \Big[\nu_* t_{r^*}^{\nu_*-1} M_2(t_{r^*}, S_h^{r^*}, E_h^{r^*}, I_h^{r^*}, R_h^{r^*}, S_v^{r^*}, E_v^{r^*}, I_v^{r^*}, T_m^{r^*}) \\
&- 2\nu_* t_{r^*-1}^{\nu_*-1} M_2(t_{r^*-1}, S_h^{r^*-1}, E_h^{r^*-1}, I_h^{r^*-1}, R_h^{r^*-1}, S_v^{r^*-1}, E_v^{r^*-1}, I_v^{r^*-1}) \\
&+ \nu_* t_{r^*-2}^{\nu_*-1} M_2(t_{r^*-2}, S_h^{r^*-2}, E_h^{r^*-2}, I_h^{r^*-2}, R_h^{r^*-2}, S_v^{r^*-2}, E_v^{r^*-2}, I_v^{r^*-2}) \Big] \\
&\times \Big[(z^*-m^*+1)^{\mu_*}[2(z^*-m^*)^2 + (3\mu_*-10)(z^*-m^*) + 2\mu_*^2 + 9\mu_* + 12] \\
&- (z^*-m^*)^{\mu_*}[2(z^*-m^*)^2 + (5\mu_*-10)(z^*-m^*) + 6\mu_*^2 + 18\mu_* + 12] \Big] .
\end{aligned}
\tag{46}
$$

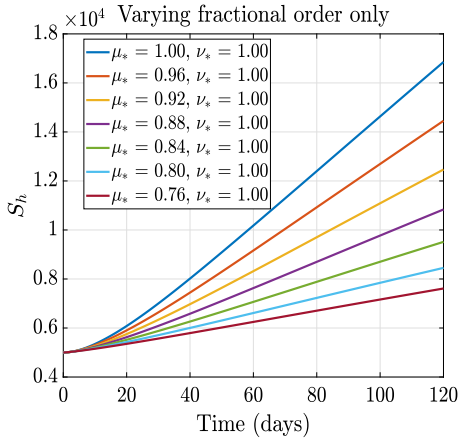

(a) Zika virus dynamics on susceptible humans

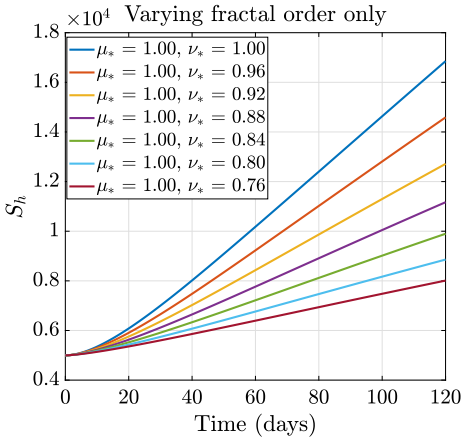

(b) Zika virus dynamics on susceptible humans

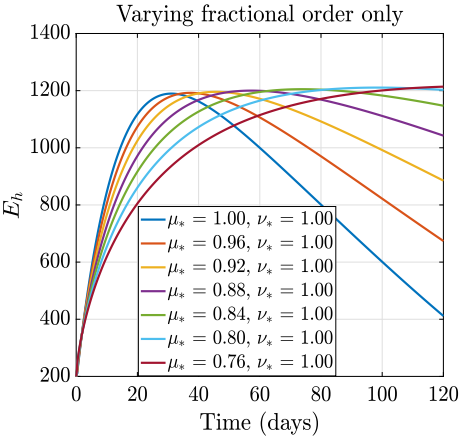

(c) Zika virus dynamics on exposed humans

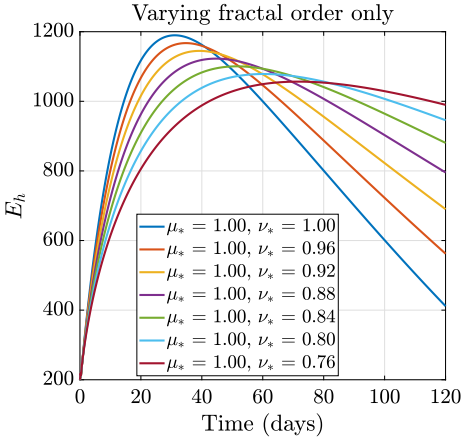

(d) Zika virus dynamics on exposed humans

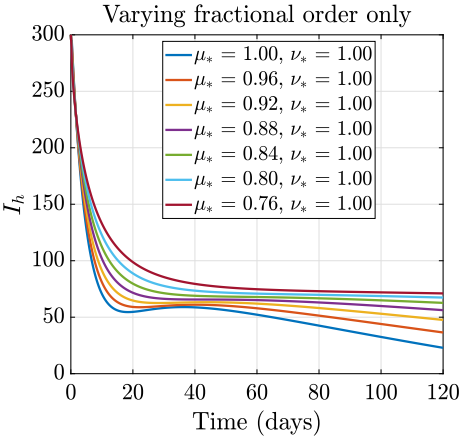

(e) Zika virus dynamics on infected humans

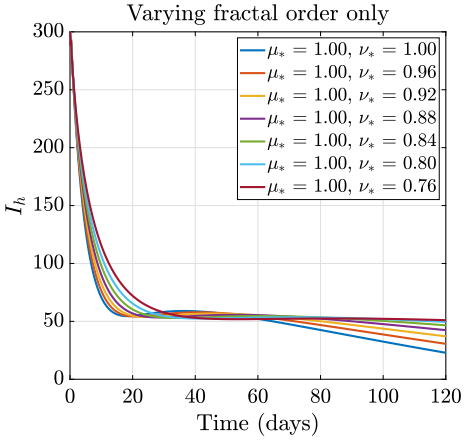

(f) Zika virus dynamics on infected humans

Fig. 3. Numerical comparison of fractional dynamics only and fractal dynamics only of the Zika transmission dynamics.

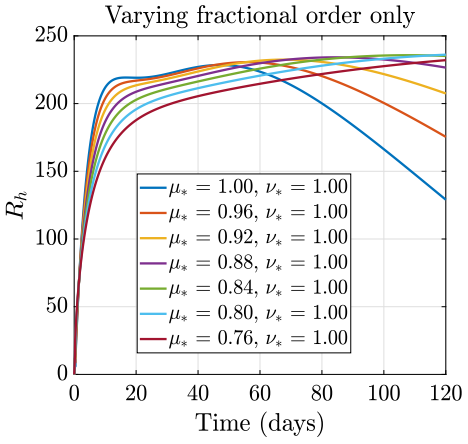

(a) Zika virus dynamics on recovered humans

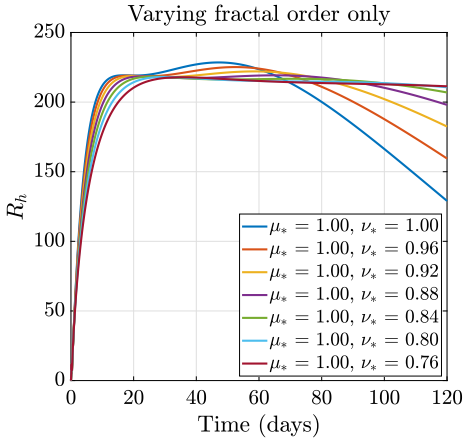

(b) Zika virus dynamics on recovered humans

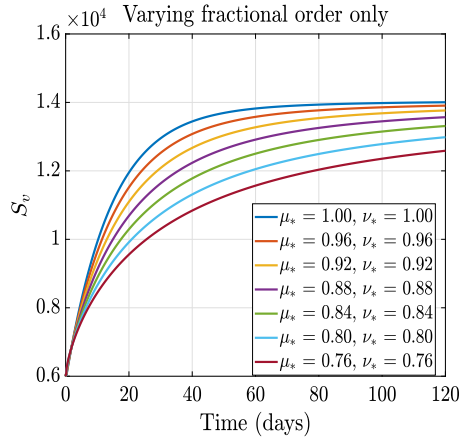

(c) Zika virus dynamics on susceptible mosquitoes

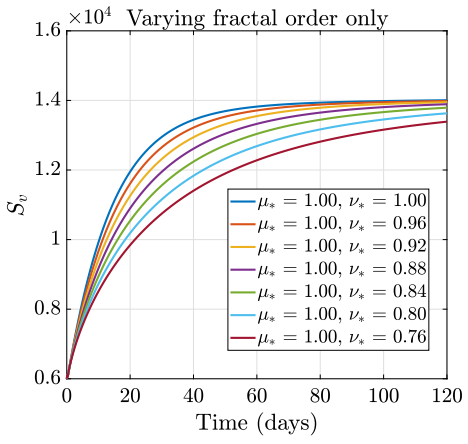

(d) Zika virus dynamics on susceptible mosquitoes

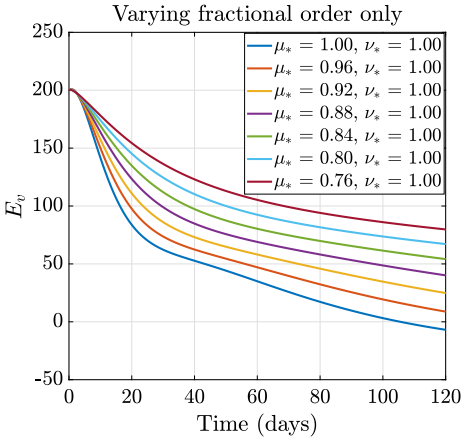

(e) Zika virus dynamics on exposed mosquitoes

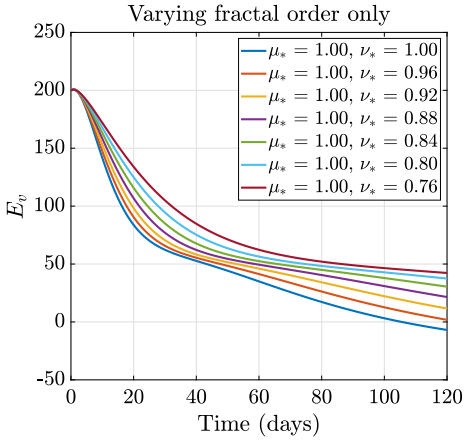

(f) Zika virus dynamics on exposed mosquitoes

Fig. 4. Numerical comparison of fractional dynamics only and fractal dynamics only of the Zika transmission dynamics.

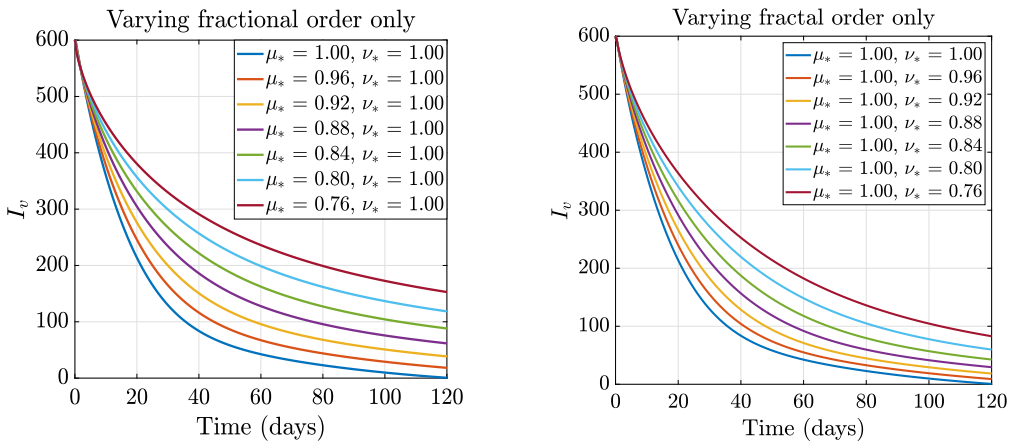

(a) Zika virus dynamics on infected mosquitoes

(b) Zika virus dynamics on infected mosquitoes

Fig. 5. Numerical comparison of fractional dynamics only and fractal dynamics only of the Zika transmission dynamics.

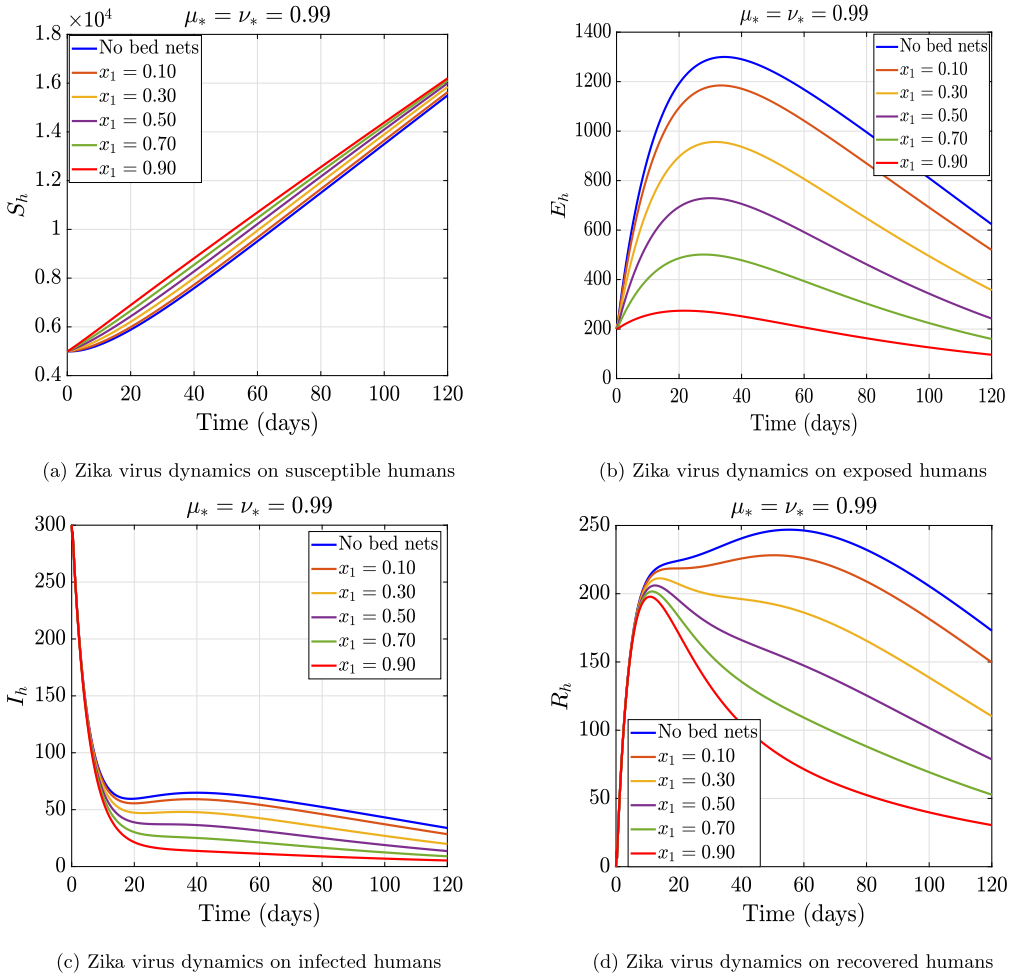

(a) Zika virus dynamics on susceptible humans

(b) Zika virus dynamics on exposed humans

(c) Zika virus dynamics on infected humans

(d) Zika virus dynamics on recovered humans

Fig. 6. Numerical dynamics of Zika transmission under the ABC fractal-fractional operator with order $\mu_* = \nu_* = 0.99$ for humans when the rate of insecticide-treated bed net coverage is changed.

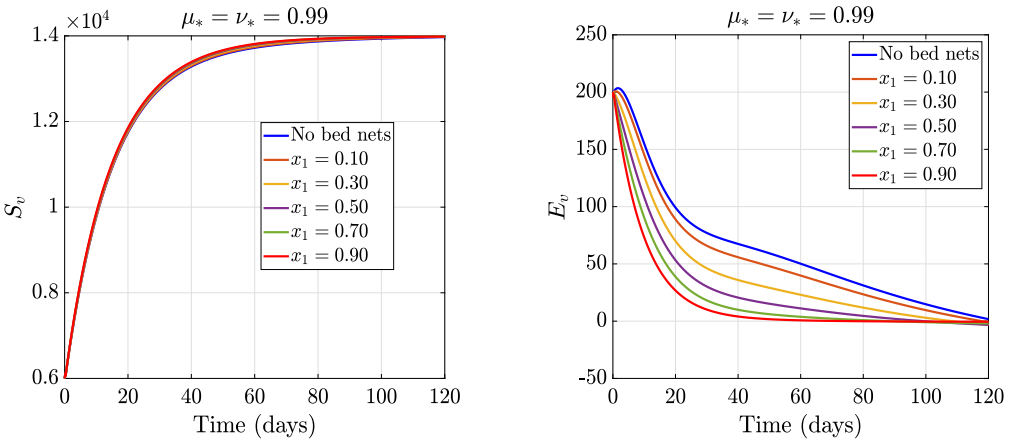

(a) Zika virus dynamics on susceptible mosquitoes

(b) Zika virus dynamics on exposed mosquitoes

(c) Zika virus dynamics on infected mosquitoes

Fig. 7. Numerical dynamics of Zika transmission under the ABC fractal-fractional operator with order $mu_* = nu_* = 0.99$ for mosquitoes when the rate of insecticide-treated net coverage is changed.

$$
\begin{aligned}
I_h^{z^*+1} &= I_h(0) + \frac{(1-\mu_*)}{\mathbf{G}(\mu_*)}\nu_* t_{z^*}^{\nu_*-1} M_3(t_n, S_h^n, E_h^n, I_h^n, R_h^n, S_v^n, E_v^n, I_v^n) + \frac{\mu_* h_*^{\mu}}{\mathbf{G}(\mu_*)\Gamma(\mu_*+1)} \\
&\sum_{r^*=2}^{z^*} \nu_* t_{r^*-2}^{\nu_*-1} M_3(t_{r^*-2}, S_h^{r^*-2}, E_h^{r^*-2}, I_h^{r^*-2}, R_h^{r^*-2}, S_v^{r^*-2}, E_v^{r^*-2}, I_v^{r^*-2}) \\
&\times \left[(z^*-m^*+1)^{\mu_*} - (z^*-m^*)^{\mu_*}\right] \\
&+ \frac{\mu_* h_*^{\mu}}{\mathbf{G}(\mu_*)\Gamma(\mu_*+2)} \sum_{r^*=2}^{z^*} \Big[\nu_* t_{r^*-1}^{\nu_*-1} M_3(t_{r^*-1}, S_h^{r^*-1}, E_h^{r^*-1}, I_h^{r^*-1}, R_h^{r^*-1}, S_v^{r^*-1}, E_v^{r^*-1}, I_v^{r^*-1}) \\
&- \nu_* t_{r^*-2}^{\nu_*-1} M_3(t_{r^*-2}, S_h^{r^*-2}, E_h^{r^*-2}, I_h^{r^*-2}, R_h^{r^*-2}, S_v^{r^*-2}, E_v^{r^*-2}, I_v^{r^*-2}) \Big] \\
&\times \left[(z^*-m^*+1)^{\mu_*}(z^*-m^*+3+2\mu_*) - (z^*-m^*)^{\mu_*}(z^*-m^*+3+3\mu_*)\right] \\
&+ \frac{\mu_* h_*^{\mu}}{2\mathbf{G}(\mu_*)\Gamma(\mu_*+3)} \sum_{r^*=2}^{z^*} \Big[\nu_* t_{r^*}^{\nu_*-1} M_3(t_{r^*}, S_h^{r^*}, E_h^{r^*}, I_h^{r^*}, R_h^{r^*}, S_v^{r^*}, E_v^{r^*}, I_v^{r^*}) \\
&- 2\nu_* t_{r^*-1}^{\nu_*-1} M_3(t_{r^*-1}, S_h^{r^*-1}, E_h^{r^*-1}, I_h^{r^*-1}, R_h^{r^*-1}, S_v^{r^*-1}, E_v^{r^*-1}, I_v^{r^*-1}) \\
&+ \nu_* t_{r^*-2}^{\nu_*-1} M_3(t_{r^*-2}, S_h^{r^*-2}, E_h^{r^*-2}, I_h^{r^*-2}, R_h^{r^*-2}, S_v^{r^*-2}, E_v^{r^*-2}, I_v^{r^*-2}) \Big] \\
&\times \Big[(z^*-m^*+1)^{\mu_*}[2(z^*-m^*)^2 + (3\mu_*-10)(z^*-m^*) + 2\mu_*^2 + 9\mu_* + 12] \\
&- (z^*-m^*)^{\mu_*}[2(z^*-m^*)^2 + (5\mu_*-10)(z^*-m^*) + 6\mu_*^2 + 18\mu_* + 12] \Big].
\end{aligned}
\tag{47}
$$

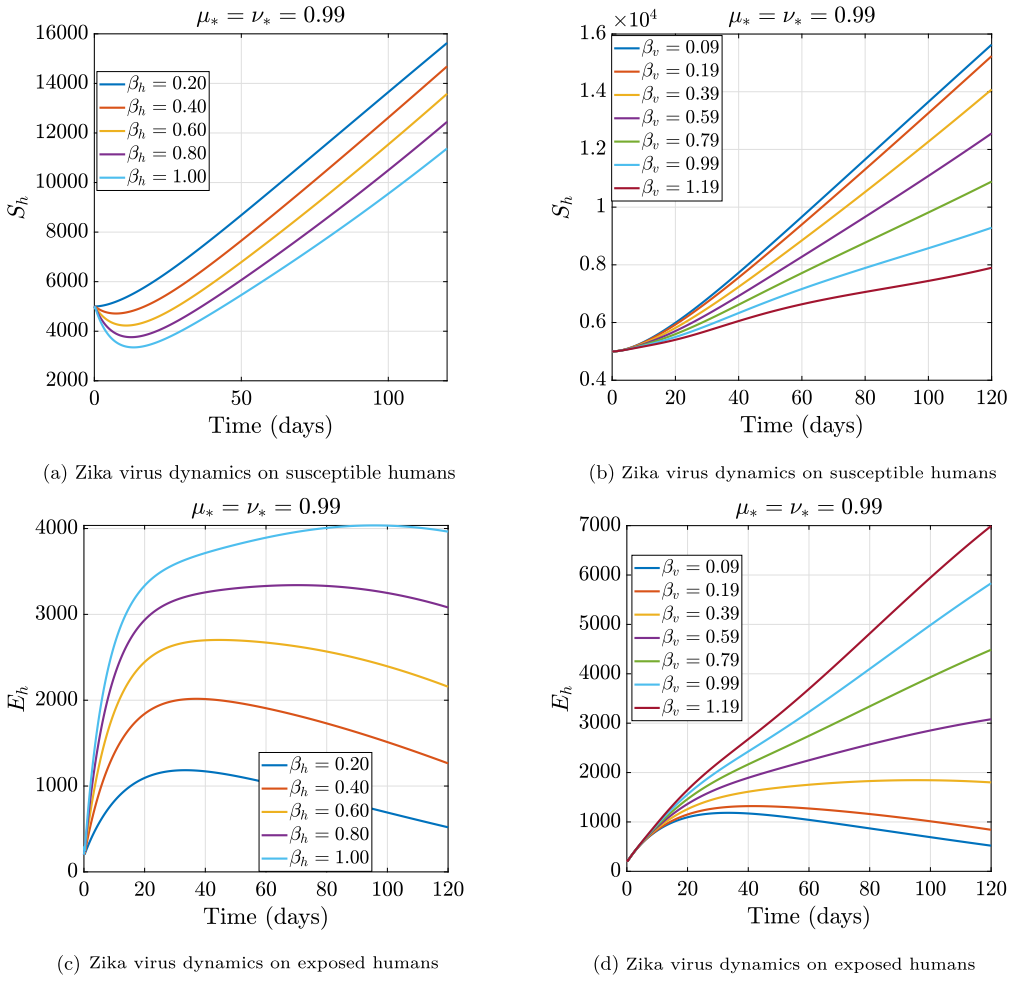

(a) Zika virus dynamics on susceptible humans

(b) Zika virus dynamics on susceptible humans

(c) Zika virus dynamics on exposed humans

(d) Zika virus dynamics on exposed humans

Fig. 8. Numerical comparison of probability of humans getting infected and probability of mosquitoes getting infected.

$$
\begin{aligned}
R_h^{z^*+1} &= R_h(0) + \frac{(1-\mu_*)}{\mathbf{G}(\mu_*)}\nu_* t_{z^*}^{\nu_*-1} M_4(t_n, S_h^n, E_h^n, I_h^n, R_h^n, S_v^n, E_v^n, I_v^n) + \frac{\mu_* h_*^{\mu}}{\mathbf{G}(\mu_*)\Gamma(\mu_*+1)} \\
&\sum_{r^*=2}^{z^*} \nu_* t_{r^*-2}^{\nu_*-1} M_4(t_{r^*-2}, S_h^{r^*-2}, E_h^{r^*-2}, I_h^{r^*-2}, R_h^{r^*-2}, S_v^{r^*-2}, E_v^{r^*-2}, I_v^{r^*-2}) \\
&\times \left[(z^*-m^*+1)^{\mu_*} - (z^*-m^*)^{\mu_*}\right] \\
&+ \frac{\mu_* h_*^{\mu}}{\mathbf{G}(\mu_*)\Gamma(\mu_*+2)} \sum_{r^*=2}^{z^*} \Big[\nu_* t_{r^*-1}^{\nu_*-1} M_4(t_{r^*-1}, S_h^{r^*-1}, E_h^{r^*-1}, I_h^{r^*-1}, R_h^{r^*-1}, S_v^{r^*-1}, E_v^{r^*-1}, I_v^{r^*-1}) \\
&- \nu_* t_{r^*-2}^{\nu_*-1} M_4(t_{r^*-2}, S_h^{r^*-2}, E_h^{r^*-2}, I_h^{r^*-2}, R_h^{r^*-2}, S_v^{r^*-2}, E_v^{r^*-2}, I_v^{r^*-2}, T_m^{r^*-2}) \Big] \\
&\times \left[(z^*-m^*+1)^{\mu_*}(z^*-m^*+3+2\mu_*) - (z^*-m^*)^{\mu_*}(z^*-m^*+3+3\mu_*)\right] \\
&+ \frac{\mu_* h_*^{\mu}}{2\mathbf{G}(\mu_*)\Gamma(\mu_*+3)} \sum_{r^*=2}^{z^*} \Big[\nu_* t_{r^*}^{\nu_*-1} M_4(t_{r^*}, S_h^{r^*}, E_h^{r^*}, I_h^{r^*}, R_h^{r^*}, S_v^{r^*}, E_v^{r^*}, I_v^{r^*}) \\
&- 2\nu_* t_{r^*-1}^{\nu_*-1} M_4(t_{r^*-1}, S_h^{r^*-1}, E_h^{r^*-1}, I_h^{r^*-1}, R_h^{r^*-1}, S_v^{r^*-1}, E_v^{r^*-1}, I_v^{r^*-1}) \\
&+ \nu_* t_{r^*-2}^{\nu_*-1} M_4(t_{r^*-2}, S_h^{r^*-2}, E_h^{r^*-2}, I_h^{r^*-2}, R_h^{r^*-2}, S_v^{r^*-2}, E_v^{r^*-2}, I_v^{r^*-2}) \Big] \\
&\times \Big[(z^*-m^*+1)^{\mu_*}[2(z^*-m^*)^2 + (3\mu_*-10)(z^*-m^*) + 2\mu_*^2 + 9\mu_* + 12] \\
&- (z^*-m^*)^{\mu_*}[2(z^*-m^*)^2 + (5\mu_*-10)(z^*-m^*) + 6\mu_*^2 + 18\mu_* + 12] \Big] .
\end{aligned}
\tag{48}
$$

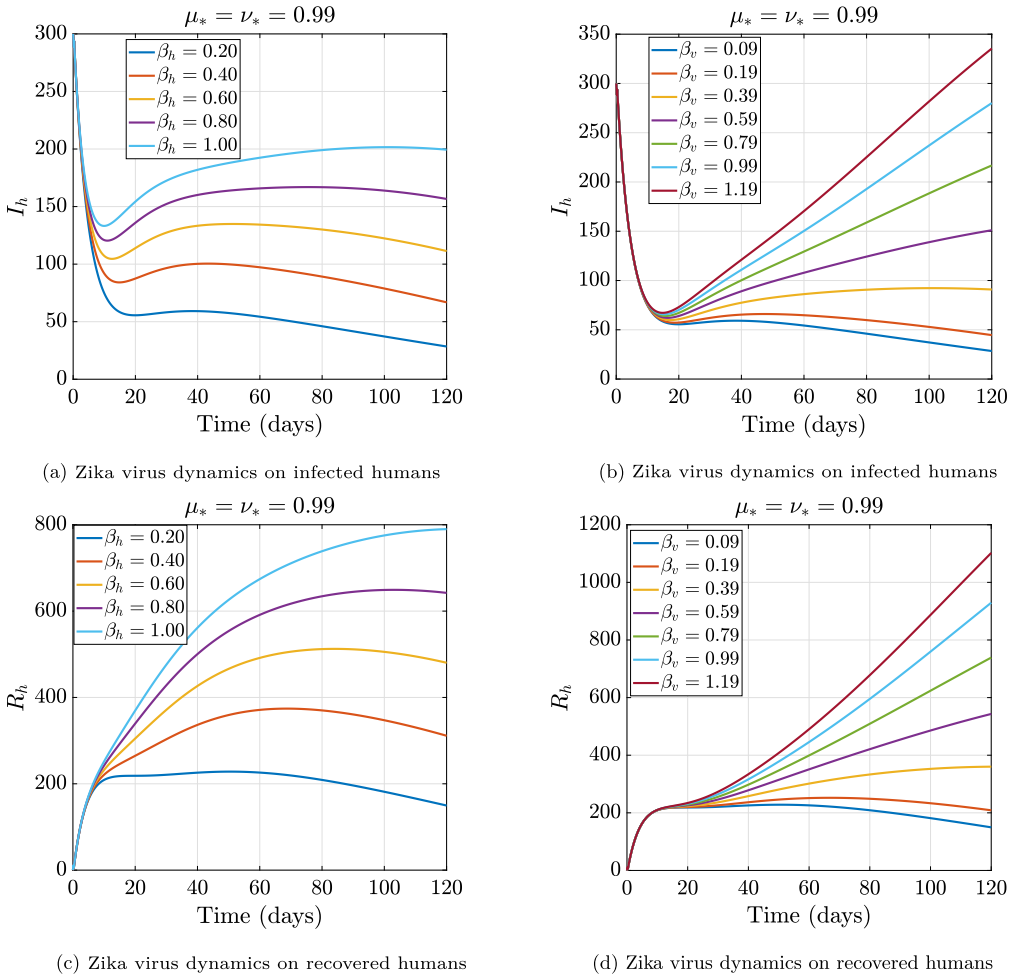

(a) Zika virus dynamics on infected humans

(b) Zika virus dynamics on infected humans

(c) Zika virus dynamics on recovered humans

(d) Zika virus dynamics on recovered humans

Fig. 9. Numerical comparison of the probability of humans getting infected and the probability of mosquitoes getting infected.

$$
\begin{aligned}
S_v^{z^*+1} &= S_v(0) + \frac{(1-\mu_*)}{\mathbf{G}(\mu_*)} \nu_* t_{z^*}^{\nu_*-1} M_5(t_n, S_h^n, E_h^n, I_h^n, R_h^n, S_v^n, E_v^n, I_v^n) + \frac{\mu_* h_*^{\mu}}{\mathbf{G}(\mu_*)\Gamma(\mu_*+1)} \\
&\sum_{r^*=2}^{z^*} \nu_* t_{r^*-2}^{\nu_*-1} M_5(t_{r^*-2}, S_h^{r^*-2}, E_h^{r^*-2}, I_h^{r^*-2}, R_h^{r^*-2}, S_v^{r^*-2}, E_v^{r^*-2}, I_v^{r^*-2}) \\
&\times \left[(z^*-m^*+1)^{\mu_*} - (z^*-m^*)^{\mu_*} \right] \\
&+ \frac{\mu_* h_*^{\mu}}{\mathbf{G}(\mu_*)\Gamma(\mu_*+2)} \sum_{r^*=2}^{z^*} \Big[\nu_* t_{r^*-1}^{\nu_*-1} M_5(t_{r^*-1}, S_h^{r^*-1}, E_h^{r^*-1}, I_h^{r^*-1}, R_h^{r^*-1}, S_v^{r^*-1}, E_v^{r^*-1}, I_v^{r^*-1}) \\
&- \nu_* t_{r^*-2}^{\nu_*-1} M_5(t_{r^*-2}, S_h^{r^*-2}, E_h^{r^*-2}, I_h^{r^*-2}, R_h^{r^*-2}, S_v^{r^*-2}, E_v^{r^*-2}, I_v^{r^*-2}) \Big] \\
&\times \left[(z^*-m^*+1)^{\mu_*}(z^*-m^*+3+2\mu_*) - (z^*-m^*)^{\mu_*}(z^*-m^*+3+3\mu_*) \right] \\
&+ \frac{\mu_* h_*^{\mu}}{2\mathbf{G}(\mu_*)\Gamma(\mu_*+3)} \sum_{r^*=2}^{z^*} \Big[\nu_* t_{r^*}^{\nu_*-1} M_5(t_{r^*}, S_h^{r^*}, E_h^{r^*}, I_h^{r^*}, R_h^{r^*}, S_v^{r^*}, E_v^{r^*}, I_v^{r^*}) \\
&- 2\nu_* t_{r^*-1}^{\nu_*-1} M_5(t_{r^*-1}, S_h^{r^*-1}, E_h^{r^*-1}, I_h^{r^*-1}, R_h^{r^*-1}, S_v^{r^*-1}, E_v^{r^*-1}, I_v^{r^*-1}) \\
&+ \nu_* t_{r^*-2}^{\nu_*-1} M_5(t_{r^*-2}, S_h^{r^*-2}, E_h^{r^*-2}, I_h^{r^*-2}, R_h^{r^*-2}, S_v^{r^*-2}, E_v^{r^*-2}, I_v^{r^*-2}) \Big] \\
&\times \Big[(z^*-m^*+1)^{\mu_*}[2(z^*-m^*)^2 + (3\mu_*-10)(z^*-m^*) + 2\mu_*^2 + 9\mu_* + 12] \\
&- (z^*-m^*)^{\mu_*}[2(z^*-m^*)^2 + (5\mu_*-10)(z^*-m^*) + 6\mu_*^2 + 18\mu_* + 12] \Big] .
\end{aligned}
\tag{49}
$$

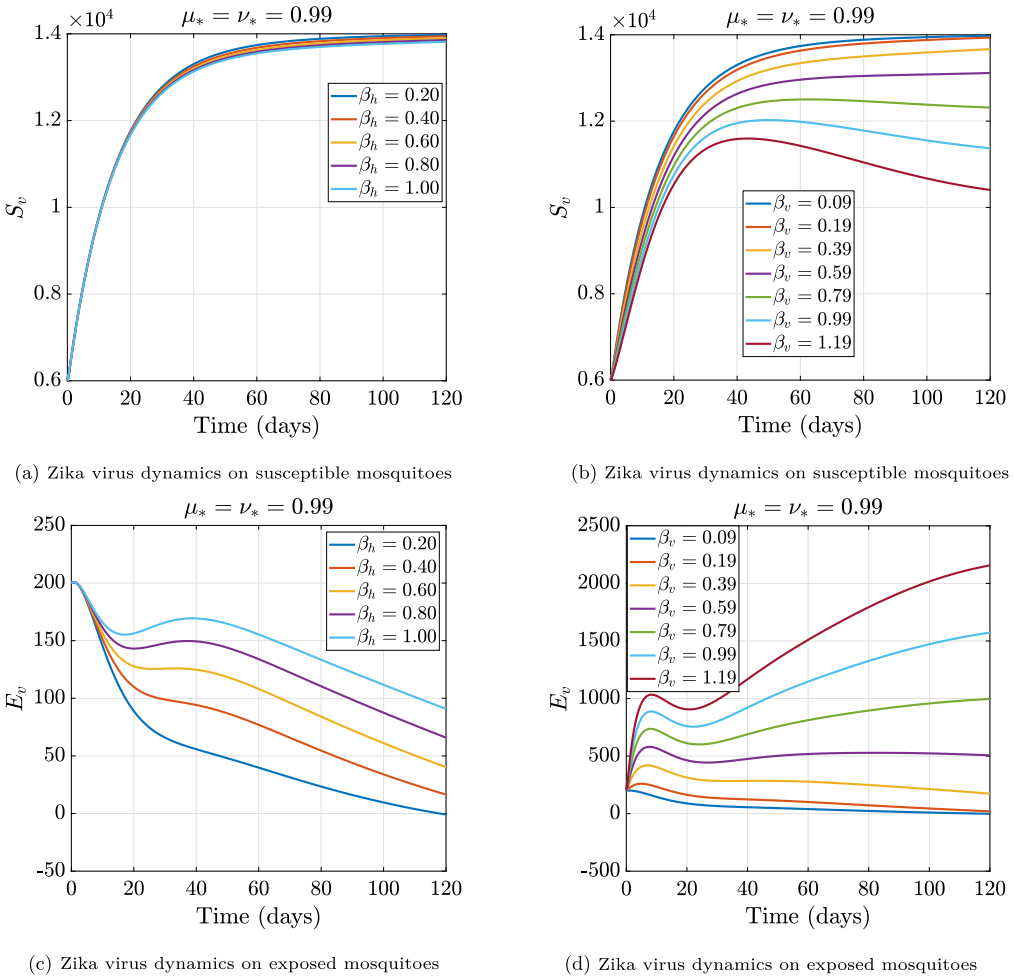

(a) Zika virus dynamics on susceptible mosquitoes

(b) Zika virus dynamics on susceptible mosquitoes

(c) Zika virus dynamics on exposed mosquitoes

(d) Zika virus dynamics on exposed mosquitoes

Fig. 10. Numerical comparison of the probability of humans getting infected and the probability of mosquitoes getting infected.

$$
\begin{aligned}
E_v^{z^*+1} &= E_V(0) + \frac{(1-\mu_*)}{\mathbf{G}(\mu_*)} \nu_* t_{z^*}^{\nu_*-1} M_6(t_n, S_h^n, E_h^n, I_h^n, R_h^n, S_v^n, E_v^n, I_v^n) + \frac{\mu_* h_*^{\mu}}{\mathbf{G}(\mu_*)\Gamma(\mu_*+1)} \\
&\sum_{r^*=2}^{z^*} \nu_* t_{r^*-2}^{\nu_*-1} M_6(t_{r^*-2}, S_h^{r^*-2}, E_h^{r^*-2}, I_h^{r^*-2}, R_h^{r^*-2}, S_v^{r^*-2}, E_v^{r^*-2}, I_v^{r^*-2}) \\
&\times \left[(z^*-m^*+1)^{\mu_*} - (z^*-m^*)^{\mu_*} \right] \\
&+ \frac{\mu_* h_*^{\mu}}{\mathbf{G}(\mu_*)\Gamma(\mu_*+2)} \sum_{r^*=2}^{z^*} \Big[\nu_* t_{r^*-1}^{\nu_*-1} M_6(t_{r^*-1}, S_h^{r^*-1}, E_h^{r^*-1}, I_h^{r^*-1}, R_h^{r^*-1}, S_v^{r^*-1}, E_v^{r^*-1}, I_v^{r^*-1}) \\
&- \nu_* t_{r^*-2}^{\nu_*-1} M_6(t_{r^*-2}, S_h^{r^*-2}, E_h^{r^*-2}, I_h^{r^*-2}, R_h^{r^*-2}, S_v^{r^*-2}, E_v^{r^*-2}, I_v^{r^*-2}, T_m^{r^*-2}) \Big] \\
&\times \left[(z^*-m^*+1)^{\mu_*}(z^*-m^*+3+2\mu_*) - (z^*-m^*)^{\mu_*}(z^*-m^*+3+3\mu_*) \right] \\
&+ \frac{\mu_* h_*^{\mu}}{2\mathbf{G}(\mu_*)\Gamma(\mu_*+3)} \sum_{r^*=2}^{z^*} \Big[\nu_* t_{r^*}^{\nu_*-1} M_6(t_{r^*}, S_h^{r^*}, E_h^{r^*}, I_h^{r^*}, R_h^{r^*}, S_v^{r^*}, E_v^{r^*}, I_v^{r^*}) \\
&- 2\nu_* t_{r^*-1}^{\nu_*-1} M_6(t_{r^*-1}, S_h^{r^*-1}, E_h^{r^*-1}, I_h^{r^*-1}, R_h^{r^*-1}, S_v^{r^*-1}, E_v^{r^*-1}, I_v^{r^*-1}) \\
&+ \nu_* t_{r^*-2}^{\nu_*-1} M_6(t_{r^*-2}, S_h^{r^*-2}, E_h^{r^*-2}, I_h^{r^*-2}, R_h^{r^*-2}, S_v^{r^*-2}, E_v^{r^*-2}, I_v^{r^*-2}) \Big] \\
&\times \Big[(z^*-m^*+1)^{\mu_*}[2(z^*-m^*)^2 + (3\mu_*-10)(z^*-m^*) + 2\mu_*^2 + 9\mu_* + 12] \\
&- (z^*-m^*)^{\mu_*}[2(z^*-m^*)^2 + (5\mu_*-10)(z^*-m^*) + 6\mu_*^2 + 18\mu_* + 12] \Big] .
\end{aligned}
\tag{50}
$$

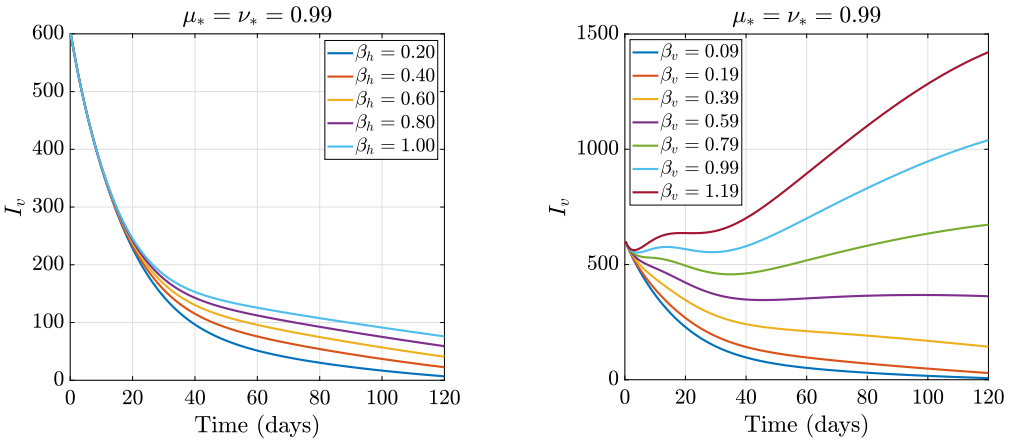

(a) Zika virus dynamics on infected mosquitoes (b) Zika virus dynamics on infected mosquitoes

Fig. 11. Numerical comparison of the probability of humans getting infected and the probability of mosquitoes getting infected.

$$
\begin{aligned}
I_v^{z^*+1} &= I_v(0) + \frac{(1-\mu_*)}{\mathbf{G}(\mu_*)} \nu_* t_{z^*}^{\nu_*-1} M_7(t_n, S_h^n, E_h^n, I_h^n, R_h^n, S_v^n, E_v^n, I_v^n) + \frac{\mu_* h_*^{\mu}}{\mathbf{G}(\mu_*)\Gamma(\mu_*+1)} \\
&\sum_{r^*=2}^{z^*} \nu_* t_{r^*-2}^{\nu_*-1} M_7(t_{r^*-2}, S_h^{r^*-2}, E_h^{r^*-2}, I_h^{r^*-2}, R_h^{r^*-2}, S_v^{r^*-2}, E_v^{r^*-2}, I_v^{r^*-2}) \\
&\times \left[(z^*-m^*+1)^{\mu_*} - (z^*-m^*)^{\mu_*}\right] \\
&+ \frac{\mu_* h_*^{\mu}}{\mathbf{G}(\mu_*)\Gamma(\mu_*+2)} \sum_{r^*=2}^{z^*} \Big[\nu_* t_{r^*-1}^{\nu_*-1} M_7(t_{r^*-1}, S_h^{r^*-1}, E_h^{r^*-1}, I_h^{r^*-1}, R_h^{r^*-1}, S_v^{r^*-1}, E_v^{r^*-1}, I_v^{r^*-1}) \\
&- \nu_* t_{r^*-2}^{\nu_*-1} M_7(t_{r^*-2}, S_h^{r^*-2}, E_h^{r^*-2}, I_h^{r^*-2}, R_h^{r^*-2}, S_v^{r^*-2}, E_v^{r^*-2}, I_v^{r^*-2}) \Big] \\
&\times \left[(z^*-m^*+1)^{\mu_*}(z^*-m^*+3+2\mu_*) - (z^*-m^*)^{\mu_*}(z^*-m^*+3+3\mu_*)\right] \\
&+ \frac{\mu_* h_*^{\mu}}{2\mathbf{G}(\mu_*)\Gamma(\mu_*+3)} \sum_{r^*=2}^{z^*} \Big[\nu_* t_{r^*}^{\nu_*-1} M_7(t_{r^*}, S_h^{r^*}, E_h^{r^*}, I_h^{r^*}, R_h^{r^*}, S_v^{r^*}, E_v^{r^*}, I_v^{r^*}) \\
&- 2\nu_* t_{r^*-1}^{\nu_*-1} M_7(t_{r^*-1}, S_h^{r^*-1}, E_h^{r^*-1}, I_h^{r^*-1}, R_h^{r^*-1}, S_v^{r^*-1}, E_v^{r^*-1}, I_v^{r^*-1}) \\
&+ \nu_* t_{r^*-2}^{\nu_*-1} M_7(t_{r^*-2}, S_h^{r^*-2}, E_h^{r^*-2}, I_h^{r^*-2}, R_h^{r^*-2}, S_v^{r^*-2}, E_v^{r^*-2}, I_v^{r^*-2}) \Big] \\
&\times \Big[(z^*-m^*+1)^{\mu_*}[2(z^*-m^*)^2 + (3\mu_*-10)(z^*-m^*) + 2\mu_*^2 + 9\mu_* + 12] \\
&- (z^*-m^*)^{\mu_*}[2(z^*-m^*)^2 + (5\mu_*-10)(z^*-m^*) + 6\mu_*^2 + 18\mu_* + 12] \Big] .
\end{aligned}
\tag{51}
$$

8. Numerical simulation and discussion

The numerical solutions and some discussions of the fractal-fractional Zika virus transmission model are presented in this section. Table 1 contains the parameters values for the numerical simulations together with the following initial conditions: $S_h(0) = 5000$; $E_h(0) = 200$; $I_h(0) = 300$; $R_h(0) = 0$; $S_v(0) = 6000$; $E_v(0) = 200$; $I_v(0) = 600$. The numerical results shown in Figs. 1, 2, 3, 4, 5, 6, 7, 8, 9, 10, and 11 represents the fractal-fractional Zika virus transmission model (11). According to the numerical simulation, when the fractional order μ_* and fractal order ν_* are reduced from 1, the number of susceptible individuals, exposed individuals, recovered individuals, and susceptible mosquitoes decreases, whereas the number of infected individuals, exposed mosquitoes, and infected mosquitoes increases in Figs. 1(c), 2(b), and 2(c), respectively. From a biological point of view, these observations suggest that as people become less aware of the disease, there could be more disease outbreaks. We also noticed crossover dynamics in Figs. 1(b) and 1(d) as the fractal-fractional order is reduced. In Figs. 3, 4 and 5 we show the numerical comparison of fractional dynamics only and fractal dynamics only of the Zika transmission dynamics. In Figs. 3(a) and 3(b), we can see that the fractional-only dynamics and fractal-only dynamics of susceptible humans are not very different. This indicates that as the memory aspect and the repeated aspect on every scale are varied with one made constant, the dynamics of the disease do not show any significant difference in the susceptible humans. In Figs. 3(c) and 3(d), we can see that the fractional-only dynamics and fractal-only dynamics

of exposed humans are different. This shows that the dynamics of the disease can vary between people who have been exposed to it since the memory aspect and the repeated aspect are different on every scale. In Figs. 3(e) and 3(f), we can see that there are no crossover dynamics in the infected humans as the fractional-only is varied, whereas there is a crossover dynamics in the infected humans from day 30 to day 75 when the fractal-only dynamics is considered. In Figs. 4(a) and 4(b), we can see crossover dynamics in the recovered humans happen after day 60, whereas there are crossover dynamics in the recovered humans from day 25 to day 75 when the fractal-only dynamics are considered. In Figs. 4(c) and 4(d), we show the dynamics of susceptible mosquitoes based on fractional only and fractal only dynamics. We noticed that when we simulated the fractional only simulation for 120 days, none of the fractional orders converged to the integer-order path, but the fractal only orders 0.96, 0.92, 0.88, and 0.84 did. In Figs. 4(e) and 4(f), we show the dynamics of exposed mosquitoes based on fractional only and fractal only dynamics. We noticed that when we simulated the fractional only simulation for 120 days, the fractional orders captured different time-space dynamics of the disease than those of the fractal only dynamics. This indicates that there is a close dynamical behaviour of the disease transmission at every repeated level of the disease rather than every memory lost aspect of the disease dynamics. In Figs. 5(a) and 5(b), we show the dynamics of infected mosquitoes based on fractional only and fractal only dynamics. We noticed that when we simulated the fractional only simulation for 120 days, the fractional orders captured more infection than those of the fractal only dynamics. This shows that forgetting about mosquitoes in the environment is a very important part of how the disease spreads.

In Figs. 6 and 7, we show the numerical sensitivity of Zika transmission for humans and mosquitos under the ABC fractal-fractional operator with order $\mu_* = \nu_* = 0.99$ when the rate of insecticide-treated bed net coverage is varied. We notice that as the rate of insecticide-treated bed net coverage increases, there is a decline in the number of exposed humans, infected humans, exposed mosquitoes, and infected mosquitoes, and a little increase in the number of susceptible humans, see Figs. 6(b), 6(c), 7(b), 7(c) and 6(a) respectively. Fig. 7(a) shows that a change in insecticide-treated bed net coverage does not result in a change in the dynamical nature of susceptible mosquitoes. Fig. 6(d) indicates that as the rate of insecticide-treated bed net coverage increases, the number of sick individuals reduces. This then results in fewer people seeking treatment to recover. In Figs. 8, 9, 10, and 11, we show the numerical sensitivity of Zika transmission for humans and mosquitos under the ABC fractal-fractional operator with order $\mu_* = \nu_* = 0.99$ when the rate of humans getting infected and the rate of mosquitos getting infected are changed. We notice that as the rate of mosquitoes getting infected increases, there is a high increase in the number individuals of each compartment of the model, see Figs. 8(b), 8(d), 9(b), 9(d), 10(b), 10(d) and 11(b) respectively, than when the rate of humans getting infected increases, see Figs. 8(a), 8(c), 9(a), 9(c), 10(a), 10(c) and 11(a) respectively. From a biological point of view, these observations suggest that a reduction in the number of infected mosquitoes' memory (fractional) and repeated patterns (fractal) of their host may reduce the Zika disease on a global scale.

9. Conclusion

In this study, we developed the transmission dynamism of the Zika virus using a fractal-fractional Zika virus transmission model incorporating insecticide-treated bed nets. The model is initially formulated via a classical integer order differential system. Then, in the first phase, we extended the Zika virus transmission model by incorporating insecticide-treated nets using the Mittag-Leffler kernel fractal-fractional derivatives. The basic mathematical properties, including boundedness, positivity, and model invariance, are explored. By means of the fixed point theorem, we proved the existence and uniqueness set of the solutions of the fractal-fractional Zika virus transmission model. We applied Hyers–Ulam stability concept to get approximate stability solution for our proposed model. In the second phase of the paper, the novel fractional-fractal Zika virus models were solved numerically using the Newton polynomial, followed by numerical simulations. The graphical representation indicated that the dynamics of fractal-fractional operators and the unique dynamism of a single operator when the other operator is kept constant. Using insecticide-treated bed net coverage shows the relative importance of controlling the dynamics of the Zika virus transmission when memory effects and repeated patterns are taken into consideration. In the future, this work could be used to study different fractal-fractional Caputo and Caputo–Fabrizio operators, and fractal-fractional optimal control of the Zika virus transmission to uncover hidden dynamics before the classical dynamics of the diseases (the integer order dynamics).

CRediT authorship contribution statement

Emmanuel Addai: Conceptualization, Methodology, Formal analysis, Writing – original draft, Writing – review & editing. **Lingling Zhang:** Supervision, Methodology, Formal analysis, Writing – review & editing. **Joseph Ackora-Prah:** Supervision, Methodology, Formal analysis, Writing – review & editing. **Joseph Frank Gordon:** Formal analysis, Writing – review & editing. **Joshua Kiddy K. Asamoah:** Supervision, Methodology, Formal analysis, Writing – original draft, Writing – review & editing. **John Fiifi Essel:** Writing – review & editing.

Declaration of competing interest

The authors declare that they have no known competing financial interests or personal relationships that could have appeared to influence the work reported in this paper.

Funding

This paper is supported by Key R&D program of Shanxi Province (International Cooperation, 201903D421042) and Research Project Supported by Shanxi Scholarship Council of China (2021-030).

References

[1] H. Nishiura, R. Kinoshita, K. Mizumoto, Y. Yasuda, K. Nah, Transmission potential of Zika virus infection in the South Pacific, Int. J. Infect. Dis. 45 (2016) 95–97, http://dx.doi.org/10.1016/j.ijid.2016.02.017.
[2] WHO, Zika Virus, https://www.who.int/news-room/fact-sheets/detail/zika-virus.
[3] CDC, Zika Virus, how the Zika virus is transmitted, https://www.cdc.gov/zika/about/overview.html.
[4] G. González-Parra, T. Benincasa, Mathematical modeling and numerical simulations of Zika in Colombia considering mutation, Math. Comput. Simulation 163 (2019) 1–18, http://dx.doi.org/10.1016/j.matcom.2019.02.009.
[5] J.K.K. Asamoah, M.A. Owusu, Z. Jin, F.T. Oduro, A. Abidemi, E.O. Gyasi, Global stability and cost-effectiveness analysis of COVID-19 considering the impact of the environment: using data from Ghana, Chaos Solitons Fractals 140 (2020) 110103, http://dx.doi.org/10.1016/j.chaos.2020.110103.
[6] N. Sene, Analysis of the stochastic model for predicting the novel coronavirus disease, Adv. Difference Equ. 2020 (1) (2020) 1–19, http://dx.doi.org/10.1186/s13662-020-03025-w.
[7] J.K.K. Asamoah, F.T. Oduro, E. Bonyah, B. Seidu, Modelling of rabies transmission dynamics using optimal control analysis, J. Appl. Math. 2017 (2017) http://dx.doi.org/10.1155/2017/2451237.
[8] J.K.K. Asamoah, Z. Jin, G.Q. Sun, Non-seasonal and seasonal relapse model for q fever disease with comprehensive cost-effectiveness analysis, Results Phys. 22 (2021) 103889, http://dx.doi.org/10.1016/j.rinp.2021.103889.
[9] A. Omame, N. Sene, I. Nometa, C.I. Nwakanma, E.U. Nwafor, N.O. Iheonu, D. Okuonghae, Analysis of COVID-19 and comorbidity co-infection model with optimal control, Optim. Control Appl. Methods 42 (6) (2021) 1568–1590.
[10] A. Abidemi, H.O. Fatoyinbo, J.K.K. Asamoah, Analysis of dengue fever transmission dynamics with multiple controls: a mathematical approach, in: 2020 International Conference on Decision Aid Sciences and Application (DASA), IEEE, 2020, pp. 971–978.
[11] A. Omame, H. Rwezaura, M.L. Diagne, S.C. Inyama, J.M. Tchuenche, COVID-19 And dengue co-infection in Brazil: optimal control and cost-effectiveness analysis, Eur. Phys. J. Plus 136 (10) (2021) 1–33.
[12] E. Acheampong, E. Okyere, S. Iddi, J.H. Bonney, J.K.K. Asamoah, J.A. Wattis, R.L. Gomes, Mathematical modelling of earlier stages of COVID-19 transmission dynamics in Ghana, Results Phys. 34 (2022) 105193.
[13] J.K.K. Asamoah, E. Yankson, E. Okyere, G.Q. Sun, Z. Jin, R. Jan, Optimal control and cost-effectiveness analysis for dengue fever model with asymptomatic and partial immune individuals, Results Phys. 31 (2021) 104919, http://dx.doi.org/10.1016/j.chaos.2020.109833.
[14] J.K.K. Asamoah, Z. Jin, G.Q. Sun, B. Seidu, E. Yankson, A. Abidemi, F.T. Oduro, S.E. Moore, E. Okyere, Sensitivity assessment and optimal economic evaluation of a new COVID-19 compartmental epidemic model with control interventions, Chaos Solitons Fractals 146 (2021) 110885, http://dx.doi.org/10.1016/j.chaos.2021.110885.
[15] B. Seidu, O.D. Makinde, Optimal control of HIV/AIDS in the workplace in the presence of careless individuals, Comput. Math. Methods Med. 2014 (2014).
[16] J.K.K. Asamoah, F. Nyabadza, Z. Jin, E. Bonyah, M.A. Khan, M.Y. Li, T. Hayat, Backward bifurcation and sensitivity analysis for bacterial meningitis transmission dynamics with a nonlinear recovery rate, Chaos Solitons Fractals 140 (2020) 110237.
[17] B. Seidu, Optimal strategies for control of COVID-19: A mathematical perspective, Scientifica 2020 (2020).
[18] J.K.K. Asamoah, Z. Jin, B. Seidu, G.Q. Sun, F.T. Oduro, F. Alzahrani, A mathematical model and sensitivity assessment of COVID-19 Outbreak for Ghana and Egypt, 2020, Available at SSRN 3612877.
[19] A. Abidemi, M.I. Abd Aziz, R. Ahmad, Vaccination and vector control effect on dengue virus transmission dynamics: Modelling and simulation, Chaos Solitons Fractals 133 (2020) 109648.
[20] S.R. Irish, H.M. Al-Amin, H.N. Paulin, A.S. Mahmood, R.K. Khan, A.K.M. Muraduzzaman, C.M. Worrell, M.S. Flora, M.J. Karim, T. Shirin, A.K.M. Shamsuzzaman, Molecular xenomonitoring for Wuchereria bancrofti in culex quinquefasciatus in two districts in Bangladesh supports transmission assessment survey findings, PLoS Negl. Trop. Dis. 12 (7) (2018) e0006574, http://dx.doi.org/10.1371/journal.pntd.0006574.
[21] L. Dinh, G. Chowell, K. Mizumoto, H. Nishiura, Estimating the subcritical transmissibility of the Zika outbreak in the State of Florida, USA, Theor. Biol. Med. Model. 13 (1) (2016) 1–7, http://dx.doi.org/10.1186/s12976-016-0046-1.
[22] A. Ali, Q. Iqbal, J.K.K. Asamoah, S. Islam, Mathematical modeling for the transmission potential of Zika virus with optimal control strategies, Eur. Phys. J. Plus 137 (1) (2022) 1–30, http://dx.doi.org/10.1140/epjp/s13360-022-02368-5.
[23] E.O. Alzahrani, W. Ahmad, M.A. Khan, S.J. Malebary, Optimal control strategies of Zika virus model with mutant, Commun. Nonlinear Sci. Numer. Simul. 93 (2021) 105532, http://dx.doi.org/10.1016/j.cnsns.2020.105532.
[24] F.B. Agusto, S. Bewick, W.F. Fagan, Mathematical model for Zika virus dynamics with sexual transmission route, Ecol. Complex. 29 (2017) 61–81, http://dx.doi.org/10.1016/j.ecocom.2016.12.007.
[25] S.C. Mpeshe, N. Nyerere, S. Sanga, Modeling approach to investigate the dynamics of Zika virus fever: A neglected disease in Africa, Int. J. Adv. Appl. Math. Mech. 4 (3) (2017) 14–21.
[26] E. Bonyah, M.A. Khan, K.O. Okosun, S. Islam, A theoretical model for Zika virus transmission, PLoS One 12 (10) (2017) e0185540.
[27] B. Tesla, L.R. Demakovsky, E.A. Mordecai, S.J. Ryan, M.H. Bonds, C.N. Ngonghala, M.A. Brindley, C.C. Murdock, Temperature drives Zika virus transmission: evidence from empirical and mathematical models, Proc. R. Soc. B 285 (1884) (2018) 20180795.
[28] A. Suparit Wiratsudakul, C. Modchang, A mathematical model for Zika virus transmission dynamics with a time-dependent mosquito biting rate, Theor. Biol. Med. Model. 15 (1) (2018) 1–11.
[29] Y. Cai, K. Wang, W. Wang, Global transmission dynamics of a Zika virus model, Appl. Math. Lett. 92 (2019) 190–195.
[30] E. Okyere, S. Olaniyi, E. Bonyah, Analysis of Zika virus dynamics with sexual transmission route using multiple optimal controls, Sci. Afr. 9 (2020) e00532.
[31] M. Chand, Z. Hammouch, J.K.K. Asamoah, D. Baleanu, Certain fractional integrals and solutions of fractional kinetic equations involving the product of S-function, in: Mathematical Methods in Engineering, Springer, Cham, 2019, pp. 213–244.
[32] W. Alhejaili, S.E. Alhazmi, R. Nawaz, A. Ali, J.K.K. Asamoah, L. Zada, Numerical investigation of Fractional–Order Kawahara and modified Kawahara equations by a semianalytical method, J. Nanomater. 2022 (2022).
[33] N. Ali, R. Nawaz, L. Zada, A. Mouldi, S.M. Bouzgarrou, N. Sene, Analytical approximate solution of the fractional order biological population model by using natural transform, J. Nanomater. 2022 (2022).
[34] D. Baleanu, A. Jajarmi, H. Mohammadi, S. Rezapour, A new study on the mathematical modelling of human liver with Caputo–Fabrizio fractional derivative, Chaos Solitons Fractals 134 (2020) 109705, http://dx.doi.org/10.1016/j.chaos.2020.109705.

[35] S.A. Khan, K. Shah, G. Zaman, F. Jarad, Existence theory and numerical solutions to smoking model under Caputo–Fabrizio fractional derivative, Chaos 29 (1) (2019) 013128, http://dx.doi.org/10.1063/1.5079644.
[36] J.K.K. Asamoah, E. Okyere, E. Yankson, A.A. Opoku, A. Adom-Konadu, E. Acheampong, Y.D. Arthur, Non-fractional and fractional mathematical analysis and simulations for Q fever, Chaos Solitons Fractals 156 (2022) 111821, http://dx.doi.org/10.1016/j.chaos.2022.111821.
[37] K.M. Owolabi, E. Pindza, Modeling and simulation of nonlinear dynamical system in the frame of nonlocal and non-singular derivatives, Chaos Solitons Fractals 127 (2019) 146–157.
[38] K.M. Owolabi, J.F. Gómez-Aguilar, B. Karaagac, Modelling, analysis and simulations of some chaotic systems using derivative with Mittag–Leffler kernel, Chaos Solitons Fractals 125 (2019) 54–63.
[39] M. Aslam, R. Murtaza, T. Abdeljawad, A. Khan, H. Khan, H. Gulzar, A fractional order HIV/AIDS epidemic model with Mittag-Leffler kernel, Adv. Difference Equ. 2021 (1) (2021) 1–15, http://dx.doi.org/10.1186/s13662-021-03264-5.
[40] M. Sher, K. Shah, Z.A. Khan, H. Khan, A. Khan, Computational and theoretical modeling of the transmission dynamics of novel COVID-19 under Mittag-Leffler power law, Alexandria Eng. J. 59 (5) (2020) 3133–3147.
[41] V.F. Morales-Delgadoa, J.F. Gomez-Aguilar, M.A. Taneco-Hernandez, R.F. Escobar-Jimenezc, V.H. Olivares-Peregrino, Mathematical modeling of the smoking dynamics using fractional differential equations with local and nonlocal kernel, J. Nonlinear Sci. Appl. 11 (8) (2018) 994–1014.
[42] A. Atangana, D. Baleanu, New fractional derivatives with nonlocal and non-singular kernel: theory and application to heat transfer model, 2016, arXiv preprint arXiv:1602.03408.
[43] A. Atangana, J.F. Gómez-Aguilar, A new derivative with normal distribution kernel: Theory, methods and applications, Physica A 476 (2017) 1–14.
[44] N. Sene, SIR Epidemic model with Mittag–Leffler fractional derivative, Chaos Solitons Fractals 137 (2020) 109833.
[45] B. Karaagac, K.M. Owolabi, K.S. Nisar, Analysis and dynamics of illicit drug use described by fractional derivative with Mittag-Leffler kernel, CMC-Comput. Mater. Cont. 65 (3) (2020) 1905–1924.
[46] K.M. Owolabi, Analysis and simulation of herd behaviour dynamics based on derivative with nonlocal and nonsingular kernel, Results Phys. 22 (2021) 103941.
[47] K.M. Owolabi, A. Atangana, Computational study of multi-species fractional reaction–diffusion system with ABC operator, Chaos Solitons Fractals 128 (2019) 280–289.
[48] L.F. Ávalos-Ruiz, J.F. Gomez-Aguilar, A. Atangana, K.M. Owolabi, On the dynamics of fractional maps with power-law, exponential decay and Mittag–Leffler memory, Chaos Solitons Fractals 127 (2019) 364–388.
[49] M.A. Khan, A. Atangana, Modeling the dynamics of novel coronavirus (2019-nCov) with fractional derivative, Alexandria Eng. J. 59 (4) (2020) 2379–2389.
[50] A. Omame, U.K. Nwajeri, M. Abbas, C.P. Onyenegecha, A fractional order control model for diabetes and COVID-19 co-dynamics with Mittag-Leffler function, Alexandria Eng. J. (2022).
[51] M.A. Khan, S. Ullah, M. Farhan, The dynamics of Zika virus with Caputo fractional derivative, AIMS Math. 4 (1) (2019) 134–146.
[52] R. Rakkiyappan, V.P. Latha, F.A. Rihan, A fractional-order model for Zika virus infection with multiple delays, Complexity 2019 (2019).
[53] M. Farman, A. Ahmad, A. Akgül, M.U. Saleem, M. Rizwan, M.O. Ahmad, A mathematical analysis and simulation for Zika virus model with time fractional derivative, Math. Methods Appl. Sci. (2020).
[54] F.M. Khan, A. Ali, Z.U. Khan, M.R. Alharthi, A.H. Abdel-Aty, Qualitative and quantitative study of Zika virus epidemic model under Caputo's fractional differential operator, Phys. Scr. 96 (12) (2021) 124030.
[55] M. Farman, A. Akgül, S. Askar, T. Botmart, A. Ahmad, H. Ahmad, Modeling and analysis of fractional order Zika model, Virus 3 (2021) 4.
[56] L.Veeresha. Akinyemi, K. Oluwasegun, M. Senol, B. Oduro, Numerical surfaces of fractional Zika virus model with diffusion effect of mosquito-borne and sexually transmitted disease, Math. Methods Appl. Sci. 45 (5) (2022) 2994–3013.
[57] A. Ali, S. Islam, M.R. Khan, S. Rasheed, F.M. Allehiany, J. Baili, M.A. Khan, H. Ahmad, Dynamics of a fractional order Zika virus model with mutant, Aej 2021 (2021) 031, http://dx.doi.org/10.1016/j.aej.2021.10.031.
[58] C. Thaiprayoon, J. Kongson, W. Sudsutad, J. Alzabut, S. Etemad, S. Rezapour, Analysis of a nonlinear fractional system for zika virus dynamics with sexual transmission route under generalized Caputo-type derivative, J. Appl. Math. Comput. (2022) 1–31.
[59] R. Begum, O. Tunç, H. Khan, H. Gulzar, A. Khan, A fractional order Zika virus model with Mittag–Leffler kernel, Chaos Solitons Fractals 146 (2021) 110898.
[60] A. Atangana, Fractal-fractional differentiation and integration: connecting fractal calculus and fractional calculus to predict complex system, Chaos Solitons Fractals 102 (2017) 396–406.
[61] K.M. Owolabi, A. Shikongo, A. Atangana, Fractal fractional derivative operator method on MCF-7 cell line dynamics, in: Methods of Mathematical Modelling and Computation for Complex Systems, Springer, Cham, 2022, pp. 319–339.
[62] A. Atangana, A. Akgül, K.M. Owolabi, Analysis of fractal fractional differential equations, Alexandria Eng. J. 59 (3) (2020) 1117–1134.
[63] K.M. Owolabi, A. Shikongo, Fractal fractional operator method on HER2+ breast cancer dynamics, Int. J. Appl. Comput. Math. 7 (3) (2021) 1–19.
[64] K.M. Owolabi, A. Atangana, A. Akgul, Modelling and analysis of fractal-fractional partial differential equations: application to reaction–diffusion model, Alexandria Eng. J. 59 (4) (2020) 2477–2490.
[65] K.M. Owolabi, E. Pindza, Numerical simulation of chaotic maps with the new generalized Caputo-type fractional-order operator, Results Phys. (2022) 105563.
[66] J.K.K. Asamoah, Fractal–fractional model and numerical scheme based on Newton polynomial for Q fever disease under Atangana–Baleanu derivative, Results Phys. (2022) 105189, http://dx.doi.org/10.1016/j.rinp.2022.105189.
[67] J.F. Gómez-Aguilar, A. Atangana, New chaotic attractors: Application of fractal-fractional differentiation and integration, Math. Methods Appl. Sci. 44 (4) (2021) 3036–3065.
[68] J.F. Gomez-Aguilar, T. Cordova-Fraga, T. Abdeljawad, A. Khan, H. Khan, Analysis of fractal–fractional malaria transmission model, Fractals 28 (08) (2020) 2040041.
[69] C.J. Zúñiga Aguilar, J.F. Gómez-Aguilar, H.M. Romero-Ugalde, H. Jahanshahi, F.E. Alsaadi, Fractal-fractional neuro-adaptive method for system identification, Eng. Comput. (2021) 1–24.
[70] K.A. Abro, A. Atangana, J.F. Gómez-Aguilar, Ferromagnetic chaos in thermal convection of fluid through fractal–fractional differentiations, J. Therm. Anal. Calorim. (2022) 1–13.
[71] H. Najafi, S. Etemad, N. Patanarapeelert, J.K.K. Asamoah, S. Rezapour, T. Sitthiwirattham, A study on dynamics of CD4+ T-cells under the effect of HIV-1 infection based on a mathematical fractal-fractional model via the Adams–Bashforth Scheme and Newton polynomials, Mathematics 10 (9) (2022) 1366.
[72] A. Atangana, Modelling the spread of COVID-19 with new fractal-fractional operators: can the lockdown save mankind before vaccination? Chaos Solitons Fractals 136 (2020) 109860.
[73] K.M. Saad, M. Alqhtani, J.F. Gómez-Aguilar, Fractal-fractional study of the hepatitis C virus infection model, Results Phys. 19 (2020) 103555.
[74] L. Zhang, M. ur Rahman, Q. Haidong, M. Arfan, Fractal-fractional anthroponotic cutaneous leishmania model study in sense of Caputo derivative, Alexandria Eng. J. 61 (6) (2022) 4423–4433.

[75] B. Zhou, L. Zhang, E. Addai, N. Zhang, Multiple positive solutions for nonlinear high-order Riemann–Liouville fractional differential equations boundary value problems with p-Laplacian operator, Bound. Value Probl. 2020 (1) (2020) 1–17.
[76] B. Zhou, L. Zhang, N. Zhang, E. Addai, Existence and monotone iteration of unique solution for tempered fractional differential equations Riemann–Stieltjes integral boundary value problems, Adv. Difference Equ. 2020 (1) (2020) 1–19.
[77] D. Musso, T. Nhan, E. Robin, C. Roche, D. Bierlaire, K. Zisou, A. Shan Yan, V.M. Cao-Lormeau, J. Broult, Potential for Zika virus transmission through blood transfusion demonstrated during an outbreak in French Polynesia, 2013 to 2014, Euro Surveill. 19 (14) (2014).
[78] M.S. Mojumder, E. Cohn, D. Fish, J.S. Brownstein, Estimating a Feasible Serial Interval Range for Zika Fever, Bull World Health Organization.
[79] O.K. Okosun, O.D. Makinde, A co-infectionmodel of malaria and cholera diseases with optimal control, Math. Biosci. 258 (2014) 19–32, pmid:25245609.
[80] E. Ahmed, A.M.A. El-Sayed, H.A. El-Saka, Equilibrium points, stability and numerical solutions of fractional-order predator–prey and rabies models, J. Math. Anal. Appl. 325 (1) (2007) 542–553.
[81] A. Granas, J. Dugundji, Fixed Point Theory, Springer-Verlag, New York, 2003.
[82] D.H. Hyers, On the stability of the linear functional equation, Proc. Natl. Acad. Sci. USA 27 (4) (1941) 222.
[83] T.M. Rassias, On the stability of the linear mapping in Banach spaces, Proc. Amer. Math. Soc. 72 (2) (1978) 297–300.
[84] A. Atangana, S.I. Araz, New Numerical Scheme with Newton Polynomial: Theory, Methods, and Applications, Academic Press, 2021.